

# On the calculation of second-order magnetic properties using subsystem approaches in the relativistic framework

Małgorzata Olejniczak\* and André Severo Pereira Gomes†

*Université de Lille, CNRS, UMR 8523 – PhLAM – Physique des Lasers,  
Atomes et Molécules, F-59000 Lille,  
France Fax: +33-3-2033-7020; Tel: +33-3-2043-4163*

Radovan Bast‡

*High Performance Computing Group,  
UiT The Arctic University of Norway,  
N-9037 Tromsø, Norway. Tel: +47-776-44117*

(Dated: January 5, 2017)

## Abstract

We report an implementation of the nuclear magnetic resonance (NMR) shielding ( $\sigma$ ), isotope-independent indirect spin-spin coupling ( $K$ ) and the magnetizability ( $\xi$ ) tensors in the frozen density embedding scheme using the four-component (4c) relativistic Dirac–Coulomb (DC) Hamiltonian and the non-collinear spin density functional theory. The formalism takes into account the magnetic balance between the large and the small components of molecular spinors and assures the gauge-origin independence of NMR shielding and magnetizability results. This implementation has been applied to hydrogen-bonded  $\text{HXH}\cdots\text{OH}_2$  complexes ( $\text{X} = \text{Se}, \text{Te}, \text{Po}$ ) and compared with the supermolecular calculations and with the approach based on the integration of the magnetically induced current density vector. A comparison with the approximate Zeroth-Order Regular Approximation (ZORA) Hamiltonian indicates non-negligible differences in  $\sigma$  and  $K$  in the  $\text{HPoH}\cdots\text{OH}_2$  complex, and calls for a thorough comparison of ZORA and DC in the description of environment effects on NMR parameters for molecular systems with heavy elements. **(Electronic Supplementary Information available at <http://dx.doi.org/10.5281/zenodo.179720>)**

---

\* gosia.olejniczak@univ-lille1.fr

† andre.gomes@univ-lille1.fr (corresponding author)

‡ radovan.bast@uit.no

## I. INTRODUCTION

The response to magnetic fields can be of great help in investigating molecular systems in complex environments. This is perhaps best illustrated by the widespread use of experimental techniques such as NMR spectroscopy to characterize compounds in condensed phase, including disordered and amorphous solids. The great sensitivity of this technique to any changes in electronic structure in the vicinity of a probed nucleus, triggered for instance by specific inter- and intramolecular interactions (e.g. hydrogen bonds) found in complex biological systems (e.g. proteins, peptides, amino acids),[1, 2] catalysts,[3] paramagnetic systems[4, 5] and radioactive compounds containing actinide atoms[6, 7] is often unrivaled by other experimental techniques.

Due to the complexity of such systems, theoretical tools can be of extreme importance to aid experimentalists interpret their results. Most theoretical approaches hinge on the recognition that, in the weak magnetic field regime under which most experiments are carried out, the magnetic field can be treated as a perturbation, the energy of a molecule can be Taylor-expanded in terms of perturbation strengths and the effect of a perturbation on a given system can be evaluated via response theory.[8]

For closed-shell systems, a static magnetic field induces only even-order changes in the total energy:[9]

$$E(\varepsilon) = E_0 + \frac{1}{2} \frac{d^2 E}{d\varepsilon_1 d\varepsilon_2} \varepsilon_1 \varepsilon_2 + \frac{1}{4!} \frac{d^4 E}{d\varepsilon_1 \dots d\varepsilon_4} \varepsilon_1 \dots \varepsilon_4 + \dots, \quad (1)$$

where  $E_0$  denotes the energy at zero field and  $\{\varepsilon_n\}$  the field strengths of applied perturbations collected in vector  $\varepsilon$ . The coefficients of this expansion, taken in the zero-field limit, define molecular properties in the Born–Oppenheimer approximation. In this paper we focus on three second-order magnetic properties arising from a perturbation of an external field  $\vec{B}$  or the field of nuclear magnetic dipole moments,  $\{\vec{m}_A\}$ : the NMR shielding tensor of a nucleus K,

$$\sigma_{\alpha\beta}^K = \left. \frac{d^2 E}{dB_\alpha dm_{K;\beta}} \right|_{\vec{B}, \{\vec{m}_A\}=0}, \quad (2)$$

the reduced spin-spin coupling tensor of nuclei K and L,

$$K_{\alpha\beta}^{KL} = \left. \frac{d^2 E}{dm_{K;\alpha} dm_{L;\beta}} \right|_{\{\vec{m}_A\}=0}, \quad (3)$$

related to the indirect spin-spin coupling constants observed in NMR experiment,  $J^{KL} = (\hbar/2\pi)\gamma_K\gamma_L K_{\alpha\beta}^{KL}$ , with  $\gamma_M$  denoting the gyromagnetic ratio of a given isotope of  $M$ , and the molecular magnetizability tensor,

$$\xi_{\alpha\beta} = -\frac{d^2 E}{dB_\alpha dB_\beta} \Big|_{\vec{B}=0}, \quad (4)$$

which, unlike the first two, is not a local but rather an extensive property as it does not depend on the magnetic moment of a given nucleus – though it may play an important role in NMR spectroscopy by inducing changes in the local magnetic fields which, in turn, will affect chemical shifts.[10–12]

NMR properties can nowadays be routinely calculated with density functional theory (DFT) for relatively large closed-shell systems and with methods based on wave function theory (WFT) for much smaller systems.[9, 13, 14] Calculating the magnetizability tensor is computationally more demanding due to the slow convergence with the basis set size. This can be partly alleviated by the use of London atomic orbitals (LAOs),[9, 15] which also remedy the gauge-origin dependence problem for properties arising from an external magnetic field perturbation  $(\xi, \sigma^K)$ , at the cost of more complex derivations and more involved implementation.

Furthermore, it is now recognized that relativistic effects[16, 17] can be appreciable for magnetizabilities[18, 19] and are essential for a proper description of NMR properties, including for those light elements neighbouring the heavy one(s) due to the so-called "heavy-atom on the light atom" (HALA) effect.[20]. NMR properties obtained with approximate Hamiltonians such as the quasirelativistic two-component (2c) ZORA Hamiltonian can differ significantly from those obtained with a more rigorous treatment afforded by four-component approaches as in the Dirac-Coulomb Hamiltonian, even for relatively light elements such as those in the fourth row of the periodic table. The conventional wisdom has been that approximate 2c approaches, which are computationally much cheaper than 4c ones, can be nevertheless reliable for relative quantities such as chemical shifts, due to error cancellation. Recent studies[21, 22] paint a more nuanced picture, and seem to indicate that there may be significant differences between Hamiltonians for relative quantities as well, notably for heavier elements.

One must also take into account the effect of the surroundings on the molecular properties, something preferably done with embedding approaches due to the steep increase in

computation cost for the explicit inclusion of e.g. solvent molecules. As methods representing the environment in an implicit manner such as PCM[23] or COSMO[24–26] have difficulty describing specific interactions such as hydrogen bonds, one is better served by approaches such as frozen-density embedding (FDE), [27–29] in which the total system is partitioned into subsystems whose interaction is calculated at DFT while the subsystems themselves can be treated with DFT (DFT-in-DFT embedding) or WFT (WFT-in-DFT embedding). FDE has been applied to the calculation of molecular properties arising from electric perturbations,[30–34] and in particular employing 4c Hamiltonians,[35, 36] though there have been only a few studies of magnetic properties: NMR shieldings[37, 38] and indirect spin-spin couplings,[39] the latter using the ZORA Hamiltonian.

The aim of this paper is therefore to bridge this gap and propose an FDE implementation that is capable of treating general second-order magnetic properties with the 4c Dirac-Coulomb (DC) Hamiltonian, by extending the general framework for response properties[30] in line with the 4c DFT simple magnetic balance (sMB) framework.[40] We also investigate the real-space determination of NMR shielding via the integration of magnetically induced currents and its use for understanding the effect of approximations introduced in practical DFT-in-DFT calculations. This will allow for investigating the suitability of approximate 2c approaches for the calculation of chemical shifts and provide a way to incorporate environment effects in the determination of shielding scales and the nuclear magnetic dipole moments,[41] a field which has received renewed interest in recent years.[42–45]

The paper is organized as follows: in the next section we present an overview of the theoretical formulation, followed by the presentation of proof-of-principle calculations on the  $\text{H}_2\text{X}-\text{H}_2\text{O}$  ( $\text{X} = \text{Se}, \text{Te}, \text{Po}$ ) family of compounds, where we also compare the description of environment effects with 2c and 4c Hamiltonians for NMR shieldings and indirect spin-spin couplings. Such a comparison for magnetizabilities is currently not possible as ours is, to the best of our knowledge, the first FDE implementation.

## II. THEORY

We begin by briefly summarizing the theory for NMR shieldings,[40, 46, 47] magnetizability[48] and NMR spin-spin couplings[46, 49, 50] in closed-shell molecules with the 4c relativistic DC Hamiltonian and mean-field methods and its implementation in the DIRAC[51] software,

followed by the general FDE framework for molecular properties[30] and its extension to magnetic properties in relativistic framework.

Throughout the text,  $i, j, \dots$  denote occupied molecular orbitals,  $a, b, \dots$  virtual orbitals and  $p, q, \dots$  orbitals in general. Greek indices are used for the three Cartesian components and Latin indices are used for the components of four-component vector. The summation over repeated indices is assumed. The SI-based atomic units are employed ( $\hbar = m_e = e = 1/(4\pi\epsilon_0) = 1$ ).[52] As we restrict ourselves to closed-shell systems represented by a single Slater determinant, we employ the following parametrization in second quantization for the unperturbed wavefunctions:

$$|\tilde{0}\rangle = \exp(-\hat{\kappa})|0\rangle; \quad \hat{\kappa} = \kappa_{ai}\hat{a}^\dagger\hat{i} - \kappa_{ai}^*\hat{i}^\dagger\hat{a}, \quad (5)$$

where  $\hat{\kappa}$  is an anti-Hermitian operator represented by a matrix of orbital rotation amplitudes, which serve as variational parameters in optimization of the ground state and its response to an external perturbation.

### A. Molecules in magnetic fields in a 4c framework

*Molecular Hamiltonian* Starting with the generic form of the Hamiltonian in the Born-Oppenheimer approximation,

$$\hat{H} = \sum_i \hat{h}_i + \sum_{i<j} \hat{g}_{ij} + V_{NN}, \quad (6)$$

with  $V_{NN}$  denoting a classical repulsion potential of clamped nuclei, it is the choice of one- and two-electron operators -  $\hat{h}_i$  and  $\hat{g}_{ij}$ , that determines whether and which relativistic effects are included.[53] The one-electron part corresponds to the Dirac operator, which in the presence of a uniform external magnetic field ( $\vec{B}$ ) and magnetic dipole moments of nuclei ( $\{\vec{m}_K\}$ ) reads:

$$\hat{h} = \hat{h}_0 + \vec{B} \cdot \hat{h}_B + \sum_K \vec{m}_K \cdot \hat{h}_{m_K}, \quad \hat{h}_0 = \beta' mc^2 + c(\vec{\alpha} \cdot \vec{p}) + v_{\text{nuc}}, \quad (7)$$

where  $\alpha$  and  $\beta' = \beta - 1_{4 \times 4}$  are  $4 \times 4$  Dirac matrices in their standard representation,  $c$  is the speed of light.[54] The Zeeman operator,  $\hat{h}_B$ , and the hyperfine operators,  $\hat{h}_{m_K}$ , are defined as:

$$\hat{h}_B = \frac{1}{2}(\vec{r}_G \times c\vec{\alpha}), \quad \hat{h}_{m_K} = \frac{1}{c^2} \frac{\vec{r}_K \times c\vec{\alpha}}{r_K^3}, \quad (8)$$

where  $\vec{r}_X = \vec{r} - \vec{R}_X$  with an arbitrary gauge origin  $\vec{R}_G$  and the center of nucleus  $K$  in  $\vec{R}_K$ . The two-electron part of the 4c DC Hamiltonian is restricted to the Coulomb potential, which in relativistic regime also includes spin-same-orbit interaction.[53]

*One-electron basis* The 4c molecular spinors, eigenfunctions of the DC Hamiltonian, are expanded in scalar finite basis sets.[54] The small component basis functions ( $\chi^S$ ) are generated from the large component functions ( $\chi^L$ ) by the restricted kinetic balance (RKB) or the restricted magnetic balance (RMB) prescription, which properly describes the relation between large and small components in the presence of external magnetic fields. The question of magnetic balance in 4c calculations was initially addressed by Aucar and coworkers [46] and Kutzelnigg,[55, 56] though later investigations have shown these yielded mixed results.[57] Later, Komorovsky and coworkers,[58–60] followed by Cheng[61] and Reynolds,[62] have revisited the question formally – and computationally – establishing RMB.

For properties explicitly dependent on an external magnetic field ( $\sigma, \xi$ ), the basis functions are replaced by London atomic orbitals,

$$\omega_\mu^K(\vec{r}) = \exp \left\{ -\frac{i}{2} \vec{B} \times (\vec{R}_K - \vec{R}_G) \cdot \vec{r} \right\} \chi_\mu^K(\vec{r}), \quad (9)$$

which guarantee the gauge-origin invariance of results in a finite basis approximation. LAOs are also appealing when used in combination with RMB as they make the magnetic balance atomic and easy to handle by the simple scheme (sMB).[40] The orthogonality of molecular orbitals at all field strengths is ensured by *connection matrices*,  $T$ , [63] which couple the unmodified molecular orbitals (UMOs) to the orthonormalized set (OMOs,  $\{\check{\psi}\}$ ),

$$\psi_q^{\text{UMO}}(\vec{B}) = \omega_\mu(\vec{B}) c_{\mu q}(0), \quad \check{\psi}_p(\vec{B}) = \psi_q^{\text{UMO}}(\vec{B}) T_{qp}(\vec{B}), \quad (10)$$

yet for the price of more complex equations, as the wave function is now dependent on a perturbation through  $\omega_\mu(\vec{B})$  and  $T(\vec{B})$  in addition to  $\kappa_{pq}(\vec{B})$ .

*Spin Density Functional Theory* The choice of the spin-density functional theory (SDFT)[64–66] is a compromise between a desirable[67–69] yet so far unattainable[70–73] DFT formalism for molecules in magnetic fields involving the current density, and the conventional charge-density-only approaches whose density functional approximations (DFAs) are developed to reproduce energy in the absence of magnetic perturbations.[74, 75] Also, due to the complexity of relativistic generalization of DFT method,[65, 76, 77] non-relativistic functionals are used with relativistic densities.

In this work, the non-collinear SDFT is employed, with the spin density (calculated as a norm of spin magnetization vector) and the charge density as basic variables, expressed together as a general density component:[40, 58, 78]

$$\rho_k(\vec{r}, \vec{B}) = \check{\Omega}_{pq;k}(\vec{r}, \vec{B}) \tilde{D}_{pq}(\kappa) \quad k \in \{0, x, y, z\}, \quad (11)$$

with the elements of the density matrix,  $\tilde{D}_{pq} = \langle \tilde{0} | p^\dagger q | \tilde{0} \rangle$  and the generalized overlap distribution,  $\check{\Omega}$ , expressed in OMO basis whenever LAOs are used:

$$\check{\Omega}_{pq;k} = \check{\psi}_p^\dagger \Sigma_k \check{\psi}_q; \quad \Sigma_0 = I_{4 \times 4}, \quad \Sigma_\mu = \begin{bmatrix} \sigma_\mu & 0_{2 \times 2} \\ 0_{2 \times 2} & \sigma_\mu \end{bmatrix}. \quad (12)$$

The ground state energy and the optimal  $\rho_k$  are obtained by minimization of the energy functional,  $E[\rho_k]$ , which can be written in a Kohn–Sham (KS) manner as a sum of five terms:

$$E[\rho_k] = T_s[\rho_k] + E_{xc}[\rho_k] + V_{NN} \quad (13)$$

$$+ \int \left( \rho_0 v_{\text{nuc}} + \sum_{\mu=x,y,z} \rho_\mu \cdot B_\mu \right) d\vec{r} + \frac{1}{2} \iint \frac{\rho_0(\vec{r}_1) \rho_0(\vec{r}_2)}{|\vec{r}_1 - \vec{r}_2|} d\vec{r}_1 d\vec{r}_2,$$

where  $T_s$  is a kinetic energy of non-interacting electrons,  $E_{xc}$  is the exchange–correlation (xc) contribution and two last terms describe the interaction of electrons with an electromagnetic potential and with other electrons, respectively. The minimization of Eq. 13 with respect to  $\rho_k$  (in the zero magnetic-field limit) yields the 4c KS equations for the DC Hamiltonian:

$$(\beta' m c^2 + c(\vec{\alpha} \cdot \vec{p}) + v_{\text{KS}}[\rho_k]) \psi = \varepsilon \psi, \quad (14)$$

with the effective KS potential :

$$v_{\text{KS}}[\rho_k] = - \left( v_{\text{nuc}} + \int \frac{\rho_0(\vec{r}')}{|\vec{r} - \vec{r}'|} d\vec{r}' + \frac{\delta E_{xc}}{\delta \rho_k} \right). \quad (15)$$

*Linear response (LR) at the 4c SDFT level* Considering now the case of time-independent perturbations with strengths  $\varepsilon_1$  and  $\varepsilon_2$ , the second-order molecular property can be written as:

$$\left. \frac{d^2 E}{d\varepsilon_1 d\varepsilon_2} \right|_{\varepsilon=0} = \left. \frac{\partial^2 E}{\partial \kappa_{pq} \partial \varepsilon_2} \frac{\partial \kappa_{pq}}{\partial \varepsilon_1} \right|_{\varepsilon=0} + \left. \frac{\partial^2 E}{\partial \varepsilon_1 \partial \varepsilon_2} \right|_{\varepsilon=0}, \quad (16)$$

assuming that the energy is optimized with respect to variational parameters at all field strengths,  $\partial E / \partial \kappa = 0$ . The first contribution is determined perturbatively, with the first-order orbital rotation amplitudes,  $\partial \kappa / \partial \varepsilon$ , obtained from the LR equations:

$$0 = \left. \frac{d}{d\varepsilon_1} \left( \frac{\partial E}{\partial \kappa_{pq}} \right) \right|_{\varepsilon=0} = \left. \left( \frac{\partial^2 E}{\partial \kappa_{pq} \partial \varepsilon_1} + \frac{\partial^2 E}{\partial \kappa_{pq} \partial \kappa_{rs}} \frac{\partial \kappa_{rs}}{\partial \varepsilon_1} \right) \right|_{\varepsilon=0}, \quad (17)$$

which can be recast in a matrix form as:[79]

$$0 = \mathbf{E}_{\varepsilon_1}^{[1]} + \mathbf{E}_0^{[2]} \mathbf{X}_{\varepsilon_1}. \quad (18)$$

Here,  $\mathbf{E}_0^{[2]}$  is the electronic Hessian,  $\mathbf{E}_{\varepsilon_1}^{[1]}$  the property gradient and  $\mathbf{X}_{\varepsilon_1}$  the solution vector yielding  $\{\kappa_{rs}^{\varepsilon_1}\}$ . While the Hessian is independent on a perturbation, the property gradient is calculated as the first-order derivative of the KS matrix with respect to field strength of applied perturbation,

$$\mathbf{E}_{\varepsilon_1}^{[1]} = \begin{bmatrix} g^{\varepsilon_1} \\ g^{*\varepsilon_1} \end{bmatrix}, \quad g_{ai}^{\varepsilon_1} = \left. \frac{\partial E_{\varepsilon_1}}{\partial \kappa_{ai}^*} \right|_0 = \langle 0 | [-\hat{a}_i^\dagger \hat{a}_a, \hat{h}_{\varepsilon_1}] | 0 \rangle = -\tilde{F}_{ai}^{\varepsilon_1}. \quad (19)$$

In particular, if  $\varepsilon_1 = \vec{B}$ , the property gradient is calculated in OMO basis and requires additional contributions involving derivatives of LAOs and of matrices T.[40, 47] Once  $\mathbf{X}_{\varepsilon_1}$  has been determined, one can construct the static linear response function:

$$\langle \langle \varepsilon_1; \varepsilon_2 \rangle \rangle_0 = E_{\varepsilon_1}^{[1]\dagger} X_{\varepsilon_2} = -E_{\varepsilon_1}^{[1]\dagger} \left( E_0^{[2]} \right)^{-1} E_{\varepsilon_2}^{[1]}, \quad (20)$$

which constitutes the response contribution to the molecular property expressed by the first term of Eq. 16. The second term of Eq. 16 can be thought of as an expectation value, which due to the linearity of the DC Hamiltonian in applied perturbations (Eq. 7) is non-zero only in perturbation-dependent basis sets.

This brings about to the final form of the properties of interest in this paper:

$$K_{\alpha\beta}^{KL} = \langle \langle m_{K;\alpha}; m_{L;\beta} \rangle \rangle_0 \quad (21)$$

$$\sigma_{\alpha\beta}^K = \langle \langle m_{K;\alpha}; B_\beta \rangle \rangle_0 \quad (22)$$

$$\xi_{\alpha\beta} = - \left( \langle \langle B_\alpha; B_\beta \rangle \rangle_0 + \left. \frac{\partial^2 E}{\partial B_\alpha \partial B_\beta} \right|_0 \right) \quad (23)$$

with the LAO basis used for the last two.

## B. Frozen Density Embedding

In FDE the total system is partitioned into interacting subsystems (for simplicity here we shall consider only two, the one of interest (I) and the other (II) representing the environment) implying a partition of the total density and energy.[27] We can further consider



the case of spin-density FDE[80, 81] and partition the generalized density component and the energy,

$$\rho_k^{\text{tot}}(\vec{r}) = \rho_k^I(\vec{r}) + \rho_k^{II}(\vec{r}) \quad (24)$$

$$E_{\text{tot}}[\rho_k^{\text{tot}}] = E_I[\rho_k^I] + E_{II}[\rho_k^{II}] + E_{\text{int}}[\rho_k^I, \rho_k^{II}], \quad (25)$$

where  $E_M[\rho_k^M]$  is the energy of an isolated subsystem ( $M = I, II$ ) calculated from Eq. 13 and  $E_{\text{int}}$  is the interaction energy dependent on densities of both subsystems,

$$\begin{aligned} E_{\text{int}}[\rho_k^I, \rho_k^{II}] &= E_{\text{tot}}[\rho_k^{\text{tot}}] - E_I[\rho_k^I] - E_{II}[\rho_k^{II}] \\ &= \int [\rho_0^I(\vec{r})v_{\text{nuc}}^{II}(\vec{r}) + \rho_0^{II}(\vec{r})v_{\text{nuc}}^I(\vec{r})] d\vec{r} + E_{\text{nuc}}^{I,II} \\ &\quad + \int \int \frac{\rho_0^I(\vec{r}_1)\rho_0^{II}(\vec{r}_2)}{|\vec{r}_1 - \vec{r}_2|} d\vec{r}_1 d\vec{r}_2 + E_{\text{xc}}^{\text{nadd}} + T_s^{\text{nadd}}. \end{aligned} \quad (26)$$

where  $E_{\text{nuc}}^{I,II}$  is the nuclear repulsion energy between subsystems,  $E_{\text{xc}}^{\text{nadd}}$  and  $T_s^{\text{nadd}}$  are the non-additive contributions defined as:[30]

$$X^{\text{nadd}} \equiv X^{\text{nadd}}[\rho_k^I, \rho_k^{II}] = X[\rho_k^{\text{tot}}] - X[\rho_k^I] - X[\rho_k^{II}]. \quad (27)$$

In order to determine  $\rho_k^I$  in the presence of other subsystem(s) with a given generalized density  $\rho_k^{II}$  one solves the 4c KS equations for a constrained electron density (KSCED)[82] which, in the limit of zero magnetic field have the form

$$(\beta' mc^2 + c(\vec{\alpha} \cdot \vec{p}) + v_{\text{KS}}[\rho_k^I] + v_{\text{emb}}^I[\rho_k^I, \rho_k^{II}]) \psi^I(\vec{r}) = \varepsilon^I \psi^I(\vec{r}), \quad (28)$$

where an effective KS potential of Eq. 15 is augmented by the embedding potential,

$$v_{\text{emb};k}^I(\vec{r}) = \frac{\delta E_{\text{int}}}{\delta \rho_k^I(\vec{r})} = \frac{\delta E_{\text{xc}}^{\text{nadd}}}{\delta \rho_k^I} + \frac{\delta T_s^{\text{nadd}}}{\delta \rho_k^I} + v_{\text{nuc}}^{II}(\vec{r}) + \int \frac{\rho_0^{II}(\vec{r}')}{|\vec{r} - \vec{r}'|} d\vec{r}', \quad (29)$$

representing the interaction of subsystem  $I$  with other subsystem(s). One can also relax the constraints on  $\rho_k^{II}$  by interchanging it with  $\rho_k^I$  and solving the analogous KSCED equations in an iterative manner in the so-called *freeze-thaw*[83] procedure.

FDE is formally exact in the limit of exact functionals describing the non-additive exchange-correlation and kinetic energies, but for computational efficiency both are generally obtained with approximate density functionals and grouped into a single term,

$$E_{\text{xck}}^{\text{nadd}}[\rho_k^I, \rho_k^{II}] = E_{\text{xc}}^{\text{nadd}}[\rho_k^I, \rho_k^{II}] + T_s^{\text{nadd}}[\rho_k^I, \rho_k^{II}]. \quad (30)$$

It should be noted that the currently available kinetic energy functionals have a limited accuracy,[27, 28] and while sufficient for relatively weak interactions (eg. hydrogen bonds),[84] practical difficulties may emerge for stronger ones requiring to replace the kinetic energy density functionals by other approaches.[85, 86]

### 1. FDE molecular properties

In what follows we shall discuss the contributions to second-order molecular properties presented in Eq. 16 in a subsystem manner. We use separate sets of externally orthogonal orbitals for subsystems  $I$  and  $II$ , [30, 87] implying the separate sets of orbital rotation coefficients,  $\kappa_{p_M q_N} = \delta_{MN} \kappa_{p_M q_M}$  for  $M, N \in \{I, II\}$ , and the parametrization of the total density (Eq. 24):

$$\rho_k^{\text{tot}}(\vec{r}, \kappa^I, \kappa^{II}) = \rho_k^I(\vec{r}, \kappa^I) + \rho_k^{II}(\vec{r}, \kappa^{II}), \quad (31)$$

with  $\kappa^M = \{\kappa_{p_M q_M}\}$  for  $M \in \{I, II\}$ .

*a. Linear response functions* The electronic Hessian and property gradient are now subdivided into isolated subsystem and interaction contributions[30]

$$\mathbf{E}_0^{[2]} = \begin{bmatrix} \mathbf{E}_0^{[2];M,M} & \mathbf{0} \\ \mathbf{0} & \mathbf{E}_0^{[2];N,N} \end{bmatrix} + \begin{bmatrix} \mathbf{E}_{0;\text{int}}^{[2];M,M} & \mathbf{E}_{0;\text{int}}^{[2];M,N} \\ \mathbf{E}_{0;\text{int}}^{[2];N,M} & \mathbf{E}_{0;\text{int}}^{[2];N,N} \end{bmatrix}, \quad (32)$$

$$\mathbf{E}_{\varepsilon_1}^{[1]} = \begin{bmatrix} \mathbf{E}_{\varepsilon_1}^{[1];M} & \mathbf{E}_{\varepsilon_1}^{[1];N} \end{bmatrix}^\dagger + \begin{bmatrix} \mathbf{E}_{\varepsilon_1;\text{int}}^{[1];M} & \mathbf{E}_{\varepsilon_1;\text{int}}^{[1];N} \end{bmatrix}^\dagger, \quad (33)$$

with  $M \neq N$ , what leads to a system of LR equations

$$(\mathbf{E}_0^{[2];M,M} + \mathbf{E}_{0;\text{int}}^{[2];M,M})\mathbf{X}_{\varepsilon_1}^M + \mathbf{E}_{0;\text{int}}^{[2];M,N}\mathbf{X}_{\varepsilon_1}^N = -(\mathbf{E}_{\varepsilon_1}^{[1];M} + \mathbf{E}_{\varepsilon_1;\text{int}}^{[1];M}), \quad (34)$$

$$\mathbf{E}_{0;\text{int}}^{[2];N,M}\mathbf{X}_{\varepsilon_1}^M + (\mathbf{E}_0^{[2];N,N} + \mathbf{E}_{0;\text{int}}^{[2];N,N})\mathbf{X}_{\varepsilon_1}^N = -(\mathbf{E}_{\varepsilon_1}^{[1];N} + \mathbf{E}_{\varepsilon_1;\text{int}}^{[1];N}), \quad (35)$$

where the response vector has also been split into blocks pertaining to each subsystem,  $\mathbf{X}_{\varepsilon_1} = [\mathbf{X}_{\varepsilon_1}^M \quad \mathbf{X}_{\varepsilon_1}^N]^\dagger$ . The matrix elements of each sub-block have the form

$$\mathbf{E}_0^{[2];M,M} = \frac{\partial^2 E_M}{\partial \kappa_{pq}^M \partial \kappa_{rs}^M}; \quad \mathbf{E}_{0;\text{int}}^{[2];M,N} = \frac{\partial^2 E_{\text{int}}}{\partial \kappa_{pq}^M \partial \kappa_{rs}^N} \quad (36)$$

for the Hessian and

$$\mathbf{E}_{\varepsilon_1}^{[1];M} = \frac{\partial^2 E_M}{\partial \kappa_{ai}^M \partial \varepsilon_1}; \quad \mathbf{E}_{\varepsilon_1;\text{int}}^{[1];M} = \frac{\partial^2 E_{\text{int}}}{\partial \kappa_{ai}^M \partial \varepsilon_1} \quad (37)$$

for the property gradient.

While the subsystem contributions to the electronic Hessian and property gradient are as in (S)DFT, the interaction contributions are calculated from the chain rule, employing the parametrization of Eq. 31, which allows for a straightforward separation of the contributions from perturbed densities of both subsystems ( $M, N \in \{I, II\}$ ):

$$\left. \frac{\partial^2 E_{\text{int}}}{\partial \kappa_{pq}^M \partial \kappa_{rs}^N} \right|_0 = \delta_{MN} \int \frac{\delta E_{\text{int}}}{\delta \rho_k^M} \frac{\partial^2 \rho_k^M}{\partial \kappa_{pq}^M \partial \kappa_{rs}^N} \Big|_0 + \iint \frac{\delta^2 E_{\text{int}}}{\delta \rho_k^M \delta \rho_{k'}^N} \frac{\partial \rho_k^M}{\partial \kappa_{pq}^M} \Big|_0 \frac{\partial \rho_{k'}^N}{\partial \kappa_{rs}^N} \Big|_0 \quad (38)$$

$$\left. \frac{\partial^2 E_{\text{int}}}{\partial \kappa_{pq}^M \partial \varepsilon_1} \right|_0 = \int \frac{\delta E_{\text{int}}}{\delta \rho_k^M} \frac{\partial^2 \rho_k^M}{\partial \kappa_{pq}^M \partial \varepsilon_1} \Big|_0 + \iint \frac{\delta^2 E_{\text{int}}}{\delta \rho_k^M \delta \rho_{k'}^N} \frac{\partial \rho_k^M}{\partial \kappa_{pq}^M} \Big|_0 \frac{\partial \rho_{k'}^N}{\partial \varepsilon_1} \Big|_0 \quad (39)$$

The functional derivatives of the interaction energy with respect to the general density components are the embedding potential  $v_{\text{emb};k}^M$  of Eq. 29 and the embedding kernel ( $M, N \in \{I, II\}$ ):

$$w_{\text{emb};k,k'}^{M,N}(\vec{r}_1, \vec{r}_2) = \frac{\delta^2 E_{\text{int}}}{\delta \rho_k^M(\vec{r}_1) \delta \rho_{k'}^N(\vec{r}_2)} = (1 - \delta_{MN}) \frac{1}{|\vec{r}_1 - \vec{r}_2|} \quad (40)$$

$$+ \frac{\delta^2 E_{\text{xck}}}{\delta \rho_k^{\text{tot}}(\vec{r}_1) \delta \rho_{k'}^{\text{tot}}(\vec{r}_2)} - \delta_{MN} \frac{\delta^2 E_{\text{xck}}}{\delta \rho_k^M(\vec{r}_1) \delta \rho_{k'}^M(\vec{r}_2)}$$

We recall that in both cases the functional derivatives are calculated with the ground-state densities.

*Electronic Hessian* The interaction energy contributions to the electronic Hessian (Eq.38) can be further rewritten as ( $M \neq N$ ):

$$\left. \frac{\partial^2 E_{\text{int}}}{\partial \kappa_{pq}^M \partial \kappa_{rs}^N} \right|_0 = \delta_{MN} \int v_{\text{emb};k}^M \frac{\partial^2 \rho_k^M}{\partial \kappa_{pq}^M \partial \kappa_{rs}^N} \Big|_0 + \iint w_{\text{emb};k,k'}^{M,M} \frac{\partial \rho_k^M}{\partial \kappa_{pq}^M} \Big|_0 \frac{\partial \rho_{k'}^M}{\partial \kappa_{rs}^M} \Big|_0 \quad (41)$$

$$+ \iint w_{\text{emb};k,k'}^{M,N} \frac{\partial \rho_k^M}{\partial \kappa_{pq}^M} \Big|_0 \frac{\partial \rho_{k'}^N}{\partial \kappa_{rs}^N} \Big|_0, \quad (42)$$

discerning the embedding potential as well as the uncoupled and coupled embedding kernel terms. In the current DIRAC implementation[30] only the terms from Eq. 41 are included, so that coupling contributions of Eq. 42 are neglected. As it is usually the case, the Hessian is not explicitly constructed but rather its eigenvectors and eigenvalues are obtained by iterative approaches.[79]

*Property gradient* When there is no dependence of  $\rho_k$  on the perturbation, Eq. 39 is identically zero and the property gradient contains only contributions from the isolated subsystems. As terms of Eq. 39 are non-zero when LAOs are used, from now on they will be referred to as FDE-LAO contributions to the property gradient. Eq. 39 can be rewritten

in a more explicit form ( $M \neq N$ ),

$$\left. \frac{\partial}{\partial B_\alpha} \frac{\partial E_{\text{int}}}{\partial \kappa_{ai}^M} \right|_0 = - \int v_{\text{emb};k}^M(\vec{r}) \check{\Omega}_{ia;k}^{B_\alpha;M} d\vec{r} \quad (43)$$

$$- \iint w_{\text{emb};k,k'}^{M,M}(\vec{r}_1, \vec{r}_2) \Omega_{ia;k}^M(\vec{r}_1) \check{\Omega}_{jj;k'}^{B_\alpha;M}(\vec{r}_2) d\vec{r}_1 d\vec{r}_2 \quad (44)$$

$$- \iint w_{\text{emb};k,k'}^{M,N}(\vec{r}_1, \vec{r}_2) \Omega_{ia;k}^M(\vec{r}_1) \check{\Omega}_{jj;k'}^{B_\alpha;N}(\vec{r}_2) d\vec{r}_1 d\vec{r}_2. \quad (45)$$

employing the notation for the embedding potential (Eq. 29), the embedding kernel (Eq. 40) and the derivatives of orbital overlap distributions (summarized in Table VI). Detailed working expressions used for practical implementation of Eq. 43-45 are presented in Appendix (Eq. 71).

Terms dependent on one subsystem, Eqs. 43-44, are in effect analogous to the XC contributions to the property gradient in OMO basis,[40] only with derivatives of the interaction energy replacing derivatives of the XC energy. In the LR algorithm[79] the property gradient is calculated once and is not updated in the iterative procedure, therefore the computational cost of including FDE-LAO terms does not significantly increase an overall cost of calculations, unless the coupling terms (Eq. 45) are considered, what will be briefly discussed in the following.

*Coupling kernel contributions to the linear response function* As terms dependent on the embedding kernel (Eq. 40) may involve perturbed densities of two different subsystems ( $M \neq N$ ), they will introduce a coupling between these subsystems through Coulomb and non-additive terms.

The coupling kernel contributions to the electronic Hessian (Eq. 42) have been discussed at length in the context of excitation energies[30, 33, 85, 88, 89] or electric polarizabilities,[34] and were shown to be important for extensive properties or when excitations cannot be considered (to good accuracy) as dominated by local components, but can often be neglected otherwise.[35–38, 90–92]

The coupling kernel contributions to the property gradient have received less attention so far. As all FDE-LAO contributions to the property gradient result from using LAOs, which shift the gauge origin from an arbitrary point to the center of nuclei, this coupling term can be regarded as a small correction due to the shift from the origin – e.g. in the center of mass of subsystem  $I$  – to the centers of nuclei in subsystem  $II$ . While we still lack the coupling contributions to the Hessian, in the following we shall nevertheless investigate the relative

importance of this term in the property gradient.

The presence of coupling terms increases the complexity and cost of calculations. As LR equations are solved for one subsystem at a time, the necessary derivatives of the density of subsystem  $II$  have to be calculated and stored before the response equations for subsystem  $I$  are invoked. Eq. 45 involves the non-additive  $E_{\text{xck}}$  term (calculated analogously as the uncoupled  $E_{\text{xck}}$  part), as well as the Coulomb contribution,

$$\int w_{\text{emb};0}^{I,II;\text{Coulomb}} \check{\Omega}_{jj;0}^{B_{\alpha};II}(\vec{r}_1) \Omega_{ia;0}^I(\vec{r}) d\vec{r}_1, \quad (46)$$

which in our implementation is calculated via numerical integration of the expression

$$\int \left[ \sum_{\mu\nu} c_{\mu i}^* c_{\nu a} \int \frac{\chi_{\mu}^{I,\dagger}(\vec{r}_1) \Sigma_0 \chi_{\nu}^I(\vec{r}_1)}{|\vec{r} - \vec{r}_1|} d\vec{r}_1 \right] \left[ \check{\Omega}_{jj;0}^{B_{\alpha};II}(\vec{r}s) \right] d\vec{r}. \quad (47)$$

*b. Expectation values* In a manner similar to the total energy in Eq. 25, the expectation value term (second term in Eq. 16) can be subdivided into subsystem and interaction parts:

$$\left. \frac{\partial^2 E}{\partial \varepsilon_1 \partial \varepsilon_2} \right|_0 = \left. \frac{\partial^2 E_I}{\partial \varepsilon_1 \partial \varepsilon_2} \right|_0 + \left. \frac{\partial^2 E_{II}}{\partial \varepsilon_1 \partial \varepsilon_2} \right|_0 + \left. \frac{\partial^2 E_{\text{int}}}{\partial \varepsilon_1 \partial \varepsilon_2} \right|_0. \quad (48)$$

The subsystem contributions will have the same form as discussed elsewhere, whereas the interaction term is

$$\left. \frac{\partial^2 E_{\text{int}}}{\partial \varepsilon_1 \partial \varepsilon_2} \right|_0 = \sum_{M=I,II} \int \frac{\delta E_{\text{int}}}{\delta \rho_k^M} \left. \frac{\partial^2 \rho_k^M}{\partial \varepsilon_1 \partial \varepsilon_2} \right|_0 \quad (49)$$

$$+ \sum_{M,N=I,II} \iint \frac{\delta^2 E_{\text{int}}}{\delta \rho_k^M \delta \rho_{k'}^N} \left. \frac{\partial \rho_k^M}{\partial \varepsilon_1} \right|_0 \left. \frac{\partial \rho_{k'}^N}{\partial \varepsilon_2} \right|_0. \quad (50)$$

From this expression one can, as in the linear response case, distinguish interaction contributions to each of subsystems,

$$\begin{aligned} \left. \frac{\partial^2 E_{\text{int}}^M}{\partial \varepsilon_1 \partial \varepsilon_2} \right|_0 &= \int \frac{\delta E_{\text{int}}}{\delta \rho_k^M} \left. \frac{\partial^2 \rho_k^M}{\partial \varepsilon_1 \partial \varepsilon_2} \right|_0 + \iint \frac{\delta^2 E_{\text{int}}}{\delta \rho_k^M \delta \rho_{k'}^M} \left. \frac{\partial \rho_k^M}{\partial \varepsilon_1} \right|_0 \left. \frac{\partial \rho_{k'}^M}{\partial \varepsilon_2} \right|_0 \\ &= \int v_{\text{emb};k}^M(\vec{r}) \check{\Omega}_{ii;k}^{B_{\alpha} B_{\beta};M} d\vec{r} \end{aligned} \quad (51)$$

$$+ \iint w_{\text{emb};k,k'}^{M,M}(\vec{r}_1, \vec{r}_2) \check{\Omega}_{ii;k}^{B_{\alpha};M}(\vec{r}_1) \check{\Omega}_{jj;k'}^{B_{\beta};M}(\vec{r}_2) d\vec{r}_1 d\vec{r}_2, \quad (52)$$

containing embedding potential and kernel contributions, and those which depend on both subsystems ( $M \neq N$ )

$$\begin{aligned} \left. \frac{\partial^2 E_{\text{int}}^{MN}}{\partial \varepsilon_1 \partial \varepsilon_2} \right|_0 &= \iint \frac{\delta^2 E_{\text{int}}}{\delta \rho_k^M \delta \rho_{k'}^N} \left. \frac{\partial \rho_k^M}{\partial \varepsilon_1} \right|_0 \left. \frac{\partial \rho_{k'}^N}{\partial \varepsilon_2} \right|_0 \\ &= \iint w_{\text{emb};k,k'}^{M,N}(\vec{r}_1, \vec{r}_2) \check{\Omega}_{ii;k}^{B_{\alpha};M}(\vec{r}_1) \check{\Omega}_{jj;k'}^{B_{\beta};N}(\vec{r}_2) d\vec{r}_1 d\vec{r}_2, \end{aligned} \quad (53)$$

made-up exclusively of a coupling kernel term. Working equations are presented in the Appendix (Eq. 73).

*Coupling kernel contributions to the expectation value* As in the case of property gradient, all terms in Eqs. 49 - 50 would be zero in perturbation-independent basis sets, thus from now on they will be referred to as FDE-LAO contributions to the expectation value. Although Eq. 53 depends on the coupling kernel, it does not involve the relaxation of the subsystems' densities as in the electronic Hessian but rather the static correction to the choice of response parameters. Here we note that first-quantization and second-quantization formulations of second-order magnetic properties in LAO basis define expectation value contributions differently.[47]

### C. Tensor Expressions for the molecular properties and their representation in terms of magnetically induced currents

The theory discussed above is sufficient to determine the properties of interest in the subsystem approach. However, these properties can also be presented in a different mathematical form using the linearity of the 4c DC Hamiltonian in applied perturbations, complemented by the formulation involving magnetically induced current densities, which more directly conveys the physical characteristics of each property.

#### 1. NMR shielding and indirect spin-spin coupling tensors

The NMR shielding or the NMR indirect spin-spin coupling tensors in Eqs. 21 and 22 can be recast in a computationally advantageous form[47] in terms of expectation values involving the hyperfine operator for a nuclei  $L$ , the unperturbed spinors  $|\psi_i\rangle$  and the first-order perturbed spinors[40, 47]  $|\tilde{\psi}_i^{\epsilon_i}\rangle$ , yielding the general expression

$$M_{\alpha\beta}^{\epsilon;L} = \sum_i \left\{ \langle \tilde{\psi}_i^{\epsilon\alpha} | \hat{h}_{m_{L;\beta}} | \psi_i \rangle + \langle \psi_i | \hat{h}_{m_{L;\beta}} | \tilde{\psi}_i^{\epsilon\alpha} \rangle \right\}. \quad (54)$$

The expression for the shielding tensor  $\sigma_{\alpha\beta}^L$  is therefore obtained from Eq. 54 by employing the spinors perturbed by the external magnetic field ( $\epsilon = \vec{B}$ ),  $|\tilde{\psi}_i^{B\alpha}\rangle$ , and by the same token the spin-spin coupling tensor  $K_{\alpha\beta}^{KL}$  is obtained by employing the spinors perturbed by the nuclear magnetic dipole ( $\epsilon = \vec{m}_K$ ),  $|\psi_i^{m_{K;\alpha}}\rangle$ .

In the FDE case, as each subsystem is described by its own set of externally-orthogonal orbitals, we can rewrite the expression in Eq. 54 as

$$M_{\alpha\beta}^{\epsilon;L} = \sum_{i \in I} \left\{ \langle \tilde{\psi}_i^{\epsilon\alpha} | \hat{h}_{m_{L;\beta}} | \psi_i \rangle + \langle \psi_i | \hat{h}_{m_{L;\beta}} | \tilde{\psi}_i^{\epsilon\alpha} \rangle \right\} \quad (55)$$

$$+ \sum_{j \in II} \left\{ \langle \tilde{\psi}_j^{\epsilon\alpha} | \hat{h}_{m_{L;\beta}} | \psi_j \rangle + \langle \psi_j | \hat{h}_{m_{L;\beta}} | \tilde{\psi}_j^{\epsilon\alpha} \rangle \right\}. \quad (56)$$

The FDE expression for  $\sigma_{\alpha\beta}^L$  or  $K_{\alpha\beta}^{KL}$  can be further approximated by neglecting the terms arising from Eq. 56. In the case of NMR shieldings, assuming nucleus  $L$  belongs to subsystem  $I$ , this approximation should be sufficient, especially if the overlap between two subsystems is small, but whatever the case we can estimate this missing contribution by the magnetically-induced current density formulation outlined in section II C 3. For the spin-spin tensor this approximation should also be good due to the local nature of the hyperfine operator, if both  $K$  and  $L$  belong to subsystem  $I$  (a restriction in our current implementation).

## 2. Magnetizability tensor

Contrary to NMR properties, the magnetizability tensor is not a local property as the Zeeman operator (Eq. 8) affects the whole system. It can be expressed in terms of the sum of (interacting) intra-subsystem and inter-subsystem contributions

$$\xi_{\alpha\beta} = \xi_{\alpha\beta}^{I,(II)} + \xi_{\alpha\beta}^{II,(I)}, \quad (57)$$

where

$$\xi_{\alpha\beta}^{I,(II)} = \left[ \frac{\partial^2 E_I}{\partial B_\alpha \partial B_\beta} \right]_0 + \left[ \frac{\partial^2 E_{\text{int}}^{M=I}}{\partial B_\alpha \partial B_\beta} \right]_0 \quad (58)$$

$$+ \left[ \frac{\partial^2 E_I}{\partial \kappa_{pq}^I \partial B_\beta} + \frac{\partial^2 E_{\text{int}}}{\partial \kappa_{pq}^I \partial B_\beta} \right] \frac{\partial \kappa_{pq}^I}{\partial B_\alpha}. \quad (59)$$

The terms in Eq. 59 are calculated by solving the linear response equations for subsystems  $I$  with FDE-LAO contributions to the property gradient (Eqs. 43 - 45). The term involving  $E_{\text{int}}^{M=I}$  in Eq. 58 will contain intra-subsystem contributions of Eqs. 51 and 52 with the summation restricted to subsystem  $I$  and the inter-subsystem contribution from Eq. 53, where the summation is constrained to have  $M = I$ . The second term in Eq. 59,  $\xi_{\alpha\beta}^{II,(I)}$ , is obtained by permutation of indices  $I$  and  $II$ .

### 3. Tensors in terms of induced currents

The relativistic current density vector and its first-order derivatives with respect to perturbations,[93]

$$\vec{j}(\vec{r}) = -e \sum_i \psi_i^\dagger c \vec{\alpha} \psi_i \quad (60)$$

$$\vec{j}^{\varepsilon_1}(\vec{r}) = -e \sum_i \left\{ \tilde{\psi}_i^{\varepsilon_1;\dagger} c \vec{\alpha} \psi_i + \psi_i^\dagger c \vec{\alpha} \tilde{\psi}_i^{\varepsilon_1} \right\}, \quad (61)$$

allow to construct property densities,[94] which may be visualized on a grid and integrated – giving the value of the corresponding property. Thus, the properties studied in this paper can be written as:

$$\sigma_{\alpha\beta}^K = -\frac{1}{c^2} \int \frac{1}{r_K^3} \left( \vec{r}_K \times \vec{j}^{B_\alpha} \right)_\beta d\vec{r}, \quad (62)$$

$$K_{\alpha\beta}^{KL} = -\frac{1}{c^2} \int \frac{1}{r_K^3} \left( \vec{r}_K \times \vec{j}^{m_{L;\alpha}} \right)_\beta d\vec{r}. \quad (63)$$

$$\xi_{\alpha\beta} = -\frac{1}{2} \int \left( \vec{r}_G \times \vec{j}^{B_\alpha} \right)_\beta d\vec{r}. \quad (64)$$

where the first-order current density perturbed by an external magnetic field is calculated with LAOs.[95]

An advantage of using the induced current density is that while evaluated for one subsystem, it can be contracted with the position vector pointing to the other subsystem allowing to evaluate contributions, for example from Eq. 56, for the NMR shielding tensor as:

$$\sigma_{\alpha\beta}^{K;II} = -\frac{1}{c^2} \int \frac{1}{(\vec{r}_i^{II} - \vec{R}_K^I)^3} \left( (\vec{r}_i^{II} - \vec{R}_K^I) \times \vec{j}^{B_\alpha;II} \right)_\beta d\vec{r}, \quad (65)$$

where the superscripts I and II denoting the subsystems are written explicitly for each vector. Eq. 65 is analogous to nucleus independent chemical shift (NICS) calculations outlined for FDE by Jacob and Visscher.[38]

### III. COMPUTATIONAL DETAILS

We have investigated three hydrogen-bonded HXH–OH<sub>2</sub> complexes, where X = Se, Te, Po. Their structures were optimized in ADF software,[96] using the scalar version of the zeroth-order regular approximation (ZORA)[97, 98] Hamiltonian, the B3LYP[99] functional and basis sets of the triple-zeta quality (TZ2P).[100] The optimized structures are included as supplementary material. The structures for the subsystems are taken from supermolecules



without any further reoptimization, so that calculation on isolated fragments can be thought of as equivalent to QM/MM embedding where only mechanical (“ME”) coupling between the subsystems is taken into account.[27]

The wave function optimization and magnetic properties calculations performed with a development version of the DIRAC code[51] employed the DC Hamiltonian and the PBE[101, 102] functional. In the FDE calculations the non-additive exchange-correlation and kinetic energy contributions were calculated with the PBE and PW91k[103] functionals, respectively. In response calculations we have used the full derivatives of the PBE and PW91k functionals provided by the XCFun library.[104] The basis sets were of augmented triple-zeta quality: aug-cc-pVTZ[105] for H and O and dyall.acv3z[106, 107] for X.

Calculations of NMR properties with the spin-orbit ZORA Hamiltonian (ZORA-SO) were performed in ADF with the TZ2P basis set and the PBE functional. For FDE calculations with ADF we have also employed the PBE and PW91k functionals for the non-additive contributions.

In both DIRAC and ADF the Gaussian model of nuclear charge distribution[108] was used and in the case of DIRAC the  $(SS|SS)$  class of two-electron integrals was replaced by a standard correction.[109] Also, in both cases we performed two sets of FDE calculations, one using densities obtained for the isolated subsystems as frozen densities (hereafter referred to as “FDE(0)”) and another where we optimized both subsystem densities by exchanging their role as frozen/active densities in the “freeze-thaw” procedure, which was stopped after 4 iterations with both densities fully optimized (hereafter referred to as “FDE(4)”). In tables in this paper we present only the latter results, while full tables are available in ESI.

We note that the choice of PBE was motivated by minimizing the differences in the computational setup between supermolecular and FDE calculations, so the only additional approximation in the FDE case comes from the kinetic energy functional. Since our aim is to compare supermolecular and FDE results, a thorough study of the performance of different functionals (exchange-correlation and/or kinetic) is beyond the scope of this paper.

We use the definitions of Mason[110] for the isotropic and the anisotropic parts of a tensor  $\Omega$  in principal axis system, where  $\Omega_{33} \geq \Omega_{22} \geq \Omega_{11}$ ,

$$\Omega_{\text{iso}} = 1/3(\Omega_{11} + \Omega_{22} + \Omega_{33}) \tag{66}$$

$$\Omega_{\text{aniso}} = \Omega_{33} - 1/2(\Omega_{11} + \Omega_{22}). \tag{67}$$

We have also calculated and plotted NMR shielding densities and their differences. In this paper we present the differential NMR shielding densities calculated by subtracting the shielding density of nucleus X and H<sub>b</sub> in Figure 1 arising from the induced current in both subsystems (employing NICS method for the frozen subsystem) from the corresponding shielding density in a supermolecule. The shielding density is plotted on a 80×80×80 grid of points generated for supermolecules. The plots were made with Mayavi - the library for interactive scientific data visualization and 3D plotting in Python.[111] More plots and relevant data can be found in ESI.

#### IV. RESULTS AND DISCUSSION

In what follows we shall present all embedding results relative to the supermolecular ones. Thus, for a given molecular property  $P$  we define absolute ( $\Delta P^f$ ) and relative ( $\delta P^f$ ) property shifts in a general manner as

$$\Delta P^f = P^{\text{super}} - (P^{I;f} + P^{II;f}) \quad (68)$$

$$\delta P^f = \Delta P^f / P^{\text{super}}, \quad (69)$$

where  $P^{\text{super}}$  corresponds to the supermolecular value of property  $P$  and  $P^{i;f}$  denotes the contribution to the property from the subsystem  $i$ . The latter is obtained for the isolated subsystem ( $f = \text{ME}$ ) or using FDE ( $f = \text{FDE}(n)$ , with  $n = 0, 4$ ). In the case of NMR shieldings and indirect spin-spin couplings, which are essentially local to one of the subsystems,  $\Delta P^f$  is well approximated by neglecting  $P^{II;f}$  in Eq. 69. In the case of FDE calculations, we introduce additional notation in order to discern FDE-LAO contributions to the property gradient (NMR shielding and magnetizability) and to the expectation value (magnetizability), which can be either neglected ( $\text{FDE}(n)[0]$ ), limited to the embedding potential ( $\text{FDE}(n)[v]$ ) or to the embedding potential and the uncoupled kernel ( $\text{FDE}(n)[v+w_u]$ ) or also incorporating the coupling kernel ( $w_c$ ) terms ( $\text{FDE}(n)[v+w_{\text{all}}]$ ).

##### A. NMR shielding tensor

The DC calculations of isotropic and anisotropic parts of NMR shielding tensor are summarized in Table I. We present only the results for nuclei of the active subsystem (H<sub>2</sub>X)

and we distinguish between the hydrogen involved in the hydrogen bond ( $H_b$ ) and the other pointing away from the water molecule.

TABLE I. Absolute DC isotropic and anisotropic shielding values ( $\sigma_{\text{iso}}^{\text{super}}$  and  $\sigma_{\text{aniso}}^{\text{super}}$ , in ppm) of nuclei in  $H_2X$  ( $X = \text{Se, Te, Po}$ ) subsystems in  $H_2X-H_2O$ , and absolute shifts ( $\Delta\sigma$ , in ppm) for the isolated (“ME”) and embedded (“FDE(4)”)  $H_2X$  molecules in the presence of  $H_2O$ . For FDE the values for different approximations in the FDE-LAO treatment ( $a : [0]$ ,  $b : [v]$ ,  $c : [v + w_u]$ ,  $d : [v + w_{\text{all}}]$ ) are shown.

Atom	$\sigma_{\text{iso}}^{\text{super}}$	$\Delta\sigma_{\text{iso}[a]}^{\text{FDE(4)}}$	$\Delta\sigma_{\text{iso}[b]}^{\text{FDE(4)}}$	$\Delta\sigma_{\text{iso}[c]}^{\text{FDE(4)}}$	$\Delta\sigma_{\text{iso}[d]}^{\text{FDE(4)}}$	$\Delta\sigma_{\text{iso}}^{\text{ME}}$
Se	2378.03	−100.75	−12.54	−12.55	−12.33	38.25
$H_b$	30.88	−0.39	−0.83	−0.67	−0.62	−2.09
H	33.42	0.24	0.02	0.03	0.03	0.43
Te	4667.85	−142.39	−4.62	−9.16	−8.88	67.48
$H_b$	35.62	−0.29	−0.68	−0.44	−0.42	−1.70
H	37.85	−0.02	0.01	0.02	0.02	0.54
Po	13985.80	−224.54	18.28	−3.52	−3.13	137.84
$H_b$	40.80	0.50	0.07	−0.09	−0.09	−0.57
H	42.29	−0.22	−0.03	0.00	0.00	0.89
	$\sigma_{\text{aniso}}^{\text{super}}$	$\Delta\sigma_{\text{aniso}[a]}^{\text{FDE(4)}}$	$\Delta\sigma_{\text{aniso}[b]}^{\text{FDE(4)}}$	$\Delta\sigma_{\text{aniso}[c]}^{\text{FDE(4)}}$	$\Delta\sigma_{\text{aniso}[d]}^{\text{FDE(4)}}$	$\Delta\sigma_{\text{aniso}}^{\text{ME}}$
Se	609.27	21.80	−0.13	−0.43	−0.19	0.17
$H_b$	22.19	5.05	6.00	5.76	5.70	7.29
H	15.13	−1.17	−0.22	−0.22	−0.21	0.09
Te	1189.67	29.78	0.56	−1.22	−1.21	3.60
$H_b$	14.59	0.50	0.02	0.24	0.28	−1.31
H	15.24	0.54	0.09	0.08	0.08	−0.64
Po	5556.67	61.88	−15.12	−18.36	−18.61	−463.51
$H_b$	105.25	0.98	−1.28	−1.67	−1.67	−6.01
H	107.80	1.93	0.16	0.08	0.09	−4.03

### 1. Isolated subsystems

From the isolated (“ME”) calculation we observe that the hydrogen-bonded water strongly affects the isotropic and anisotropic parts of the NMR shielding tensors of nuclei of the active subsystems, leading to the shielding of the heavy centers and the deshielding of  $H_b$ , in agreement with established observations on hydrogen-bonded systems.[112]

The values of  $\Delta\sigma_{\text{iso}}^{\text{ME}}$  are progressively larger with the increase of atomic number of X for all nuclei of an active subsystem: for the X nuclei they range from 38 ppm for  $\text{SeH}_2$  to 138 ppm for  $\text{PoH}_2$ , for the non H-bonded hydrogen nuclei – from 0.4 ppm for  $\text{SeH}_2$  to 0.9 ppm for  $\text{PoH}_2$  and for  $H_b$  nuclei – from –2 ppm for  $\text{SeH}_2$  to –0.6 ppm for  $\text{PoH}_2$ , which for hydrogen nuclei are significant since  $^1\text{H}$  NMR shielding is between 10 ppm and 30 ppm in most applications.[14]

While these  $\Delta\sigma$  values are relatively small in comparison to the absolute shieldings, they can nevertheless be significant in NMR experiments – for instance, both  $^{77}\text{Se}$  and  $^{125}\text{Te}$  nuclei are known to be very sensitive to the environment (e.g. solvent, its concentration and temperature[113]) and even though they span wide chemical shift ranges (6000 ppm for  $^{77}\text{Se}$ [114, 115] and 7000 ppm[113] for  $^{125}\text{Te}$ ), shifts of around 30 ppm (Se) or 60 ppm (Te) are fingerprints of a specific solvent.[113, 116–118]

For the anisotropies, isolated (“ME”) results are usually very different than the supermolecular ones for  $H_b$ , with  $\Delta\sigma_{\text{aniso}}^{\text{ME}}$  of 7 ppm for  $\text{SeH}_2$ , –1 ppm for  $\text{TeH}_2$  and –6 ppm for  $\text{PoH}_2$ , which represent deviations of 33%, 9% and 6% respectively. This is not unexpected, since in order to properly capture the directionality of the hydrogen bond, electronic effects must be taken into account. Interestingly, these discrepancies are also seen for the Po nucleus in  $\text{PoH}_2$ , whose shielding anisotropy differs from the supermolecular value by 464 ppm (or 8% difference to the supermolecular value), whereas no significant deviations are seen for Se or Te.

These tendencies can be better seen in the plots of the differential isotropic shielding density in Figure 1 (a) for the heavy centers and  $H_b$ . Those figures exhibit positive (pink) and negative (blue) isosurfaces, which, respectively, depict more shielded and more deshielded areas in a supermolecule than in the embedded subsystems, and which upon integration give the corresponding values of  $\Delta\sigma_{\text{iso}}^{\text{ME}}$ .

We observe from Figure 1 (a) that the plots are rather similar for Se and Te nuclei,

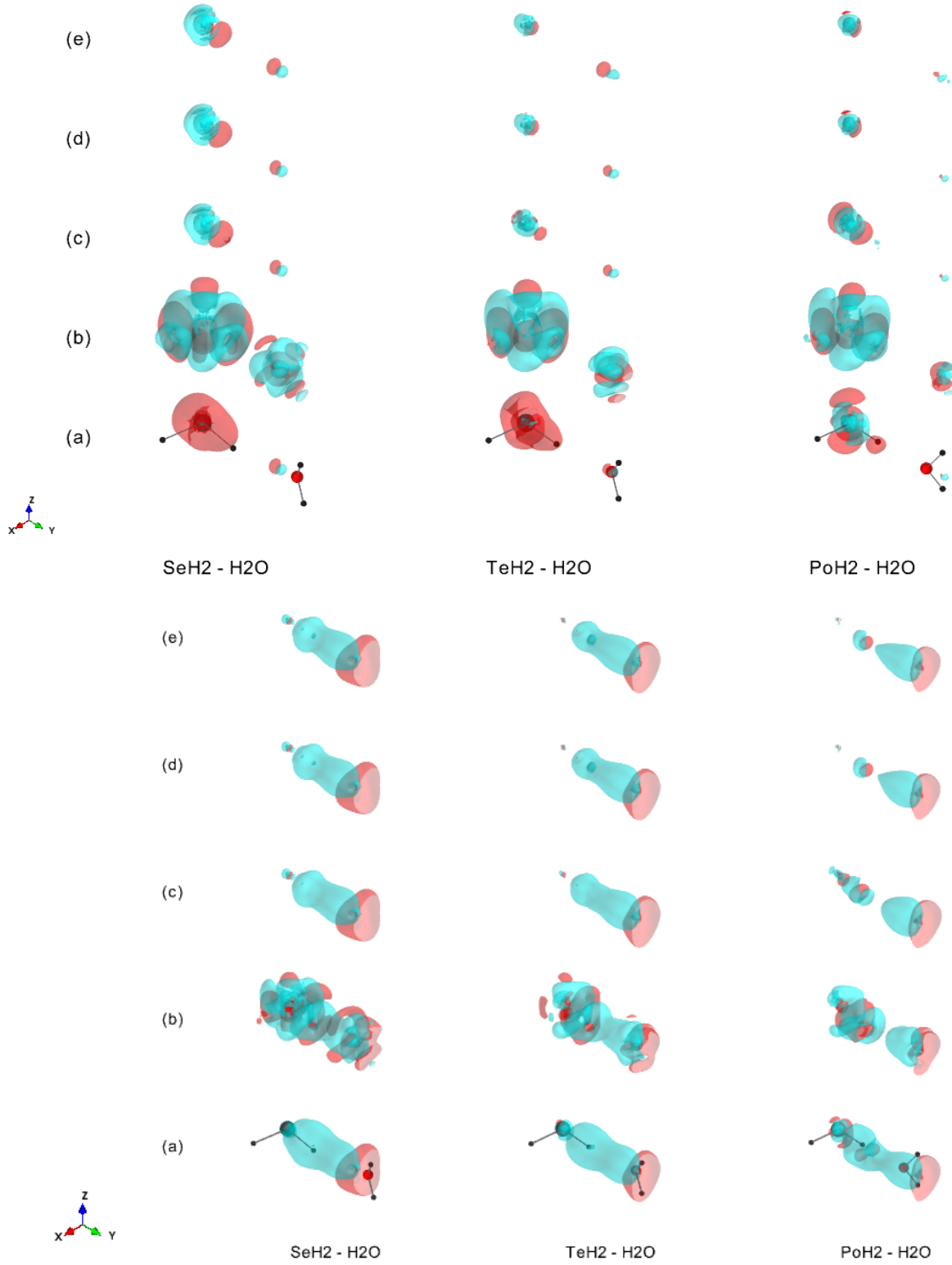


FIG. 1. Differential isotropic shielding density isosurfaces[119] (isovalues at +0.53 ppm (red) and -0.53 ppm (blue)) for  $\text{XH}_2 - \text{H}_2\text{O}$  systems  $\text{X} = \text{Se}, \text{Te}, \text{Po}$  (top) and  $\text{H}_b$  (bottom), calculated as a difference between supermolecule shielding densities and the sum of subsystem shielding densities approximated as: (a) ME (b) FDE(4)[0] (c) FDE(4)[v] (d) FDE(4)[v+w<sub>u</sub>] (e) FDE(4)[v+w<sub>all</sub>]. Color of atoms: X (blue), O (red), H (grey).

exhibiting small negative isosurfaces centered on a heavy nucleus, surrounded by much larger positive isosurface elongated on X-H<sub>b</sub> bond. In case of Po the differential shielding density is represented by much more complex isosurfaces around heavy center, as the negative isosurface centered on Po is larger than observed for Se and Te and surrounded by many well-separated positive lobes. This indicates that even though the property shift  $\Delta\sigma_{\text{iso}}^{\text{ME}}(\text{Po})$  turns out to be relatively modest compared to the value of the absolute shielding, it is a result of shielded and deshielded areas cancelling out upon integration, reflecting the intricate interplay between environmental and relativistic effects, which are quite different for Te and Se.

Towards the heavier neighbouring center, hydrogen nuclei experience larger HALA effects[120] (reflected by increasing absolute values of  $\sigma_{\text{iso}}^{\text{super}}(\text{H}_b)$ ) contributing to the shielding of H<sub>b</sub> nuclei, and competing with the deshielding effect caused by the interaction with water molecule. We also observe the difference in the non hydrogen bonded hydrogen shielding between PoH<sub>2</sub> and the other species, which could also be a consequence of the HALA effect.

## 2. Frozen Density Embedding

In what follows we discuss the relative importance of the FDE-LAO contributions ( $v, w_u, w_c$ ), both in terms of the values of isotropic and anisotropic  $\Delta\sigma^{\text{FDE(4)}}$  indices as well as from the plots of the differential isotropic shielding density in Figure 1 (b)-(e). We also calculated contributions to shielding of X and H<sub>b</sub> from the frozen subsystem using the induced current density formulation from Eq. 65, but since for all approximations these were found to be smaller than the assumed accuracy (0.01 ppm), they are not shown separately.

Starting with the calculation where no FDE-LAO terms are added to the property gradient, the results of isotropic shieldings are much worse than the “ME” values for all nuclei considered. The same conclusion is drawn for anisotropic shieldings of Se and Te nuclei, but not for Po nucleus, for which  $\Delta\sigma_{\text{aniso}}^{\text{FDE(4)}}$  value remains smaller than the one incorporating only the mechanical coupling.

The inclusion of FDE-LAO[ $v$ ] contributions yields significant improvement over the isolated values. For the heavy elements,  $\Delta\sigma_{\text{iso}}^{\text{FDE(4)}}$  increases from the very negative values obtained without FDE-LAO terms to still significant negative values for Se (−13 ppm), less

negative for Te (−4 ppm) and positive for Po (18 ppm). For  $H_b$  the inclusion of the potential acts in the opposite direction and we observe relatively small decrease of  $\Delta\sigma_{\text{iso}}^{\text{FDE}(4)}$  values, whereas for the other hydrogen there is little change.

Uncoupled kernel contributions ( $v + w_u$ ) further improve results as they partially offset the  $v$  contribution and reduce the  $\Delta\sigma_{\text{iso}}^{\text{FDE}(4)}$  to rather small values. The  $w_u$  correction is much more significant for Po than for Te, and for Se only little improvement is seen. The reason for this difference among elements is that the kernel terms introduce contributions from the response of the spin-density which becomes more significant as the elements become heavier. This is also the reason why  $w_u$  contributions affect the shielding of  $H_b$  atoms (spin-orbit mechanism of HALA effect). The uncoupled kernel also accentuates the trend seen for  $\Delta\sigma_{\text{aniso}}^{\text{FDE}(4)}(\text{X})$ , making it more negative and therefore overestimating shielding anisotropy of X. This overestimation is also observed for the  $\sigma_{\text{aniso}}^{\text{FDE}(4)}(H_b)$  except in  $\text{SeH}_2$ .

The coupling terms ( $w_c$ ), on the other hand, act in general to offset the uncoupled kernel terms but their magnitude is, as expected from the local nature of the NMR shielding, much smaller than the latter for all atoms so it plays no significant role in either the isotropic shielding value or the shielding anisotropy.

All of the above let us conclude that, while FDE isotropic shieldings are rather good and relatively much better as the systems become heavier, there are still significant shortcomings in the description of the anisotropies in these systems. The key to further improve the results is in ameliorating the leading FDE-LAO contribution ( $v$ ), and a possible way to do so is via the use of accurate approximations to the non-additive kinetic energy contributions.[85, 86]

## B. Magnetizability

The magnetizability tensors calculated with the DC Hamiltonian are summarized in Table II, where we present the isotropic ( $\xi_{\text{iso}}$ ) and first anisotropy ( $\xi_{\text{aniso1}}$ ) values. The results for the second anisotropy,  $\xi_{\text{aniso2}}$ , can be found in the supplementary material.

The magnetizability is an extensive property and therefore in order to compare to the supermolecular values one should obtain the tensors for both subsystems. Another of its features, demonstrated by numerous studies, is that its value in a molecule can be very well approximated by a sum of contributing atomic susceptibilities,[121–123] with only few exceptions, e.g. aromatic hydrocarbons,[123] small molecules containing fluorine[124] or

TABLE II. DC isotropic and first anisotropic magnetizabilities ( $\xi_{\text{iso}}$  and  $\xi_{\text{aniso1}}$ , in SI units) for the  $\text{H}_2\text{X}-\text{H}_2\text{O}$  ( $\text{X} = \text{Se}, \text{Te}, \text{Po}$ ) systems as well as for the  $\text{H}_2\text{X}$  and  $\text{H}_2\text{O}$  subsystems, the latter as isolated (“ME”) and embedded (“FDE(4)”) calculations. In the case of subsystem calculations the total  $\xi_{\text{iso}}^{\text{tot}}$  and  $\xi_{\text{aniso1}}^{\text{tot}}$  are given as the sum of the subsystem values. For FDE the values for the different approximations in the FDE-LAO treatment ( $a : [0], b : [v], c : [v + w_u], d : [v + w_{\text{all}}]$ ) are shown.

System	$\xi_{\text{iso}}^{\text{super}}$	$\xi_{\text{iso[a]}}^{\text{FDE(4)}}$	$\xi_{\text{iso[b]}}^{\text{FDE(4)}}$	$\xi_{\text{iso[c]}}^{\text{FDE(4)}}$	$\xi_{\text{iso[d]}}^{\text{FDE(4)}}$	$\xi_{\text{iso}}^{\text{ME}}$
SeH <sub>2</sub>	—	−183.07	−608.99	−606.54	−606.54	−602.19
H <sub>2</sub> O	—	781.33	−233.79	−233.78	−233.76	−234.19
$\xi^{\text{tot}}$	−836.26	598.26	−842.77	−840.32	−840.30	−836.31
$\Delta\xi$	0.0	−1434.52	6.51	4.06	4.04	0.05
TeH <sub>2</sub>	—	−630.07	−858.94	−848.68	−848.74	−842.57
H <sub>2</sub> O	—	235.10	−233.74	−233.74	−233.60	−233.83
$\xi^{\text{tot}}$	−1080.67	−394.97	−1092.69	−1082.42	−1082.33	−1076.39
$\Delta\xi$	0.0	−685.71	12.01	1.74	1.66	−4.28
PoH <sub>2</sub>	—	−895.55	−1030.19	−949.80	−949.71	−940.09
H <sub>2</sub> O	—	−169.52	−234.11	−234.10	−233.18	−234.02
$\xi^{\text{tot}}$	−1184.04	−1065.08	−1264.30	−1183.91	−1182.89	−1174.11
$\Delta\xi$	0.0	−118.96	80.26	−0.13	−1.15	−9.92
	$\xi_{\text{aniso1}}^{\text{super}}$	$\xi_{\text{aniso1[a]}}^{\text{FDE(4)}}$	$\xi_{\text{aniso1[b]}}^{\text{FDE(4)}}$	$\xi_{\text{aniso1[c]}}^{\text{FDE(4)}}$	$\xi_{\text{aniso1[d]}}^{\text{FDE(4)}}$	$\xi_{\text{aniso1}}^{\text{ME}}$
SeH <sub>2</sub>	—	−358.80	−47.12	−45.88	−45.88	−45.97
H <sub>2</sub> O	—	−1396.29	−5.76	−5.76	−5.78	−6.51
$\xi^{\text{tot}}$	−57.94	−1755.08	−52.88	−51.64	−51.66	−52.48
$\Delta\xi$	0.0	1697.14	−5.07	−6.31	−6.28	−5.47
TeH <sub>2</sub>	—	−227.24	−86.32	−80.29	−80.32	−80.30
H <sub>2</sub> O	—	−650.52	−5.53	−5.53	−5.70	−6.06
$\xi^{\text{tot}}$	−81.63	−877.77	−91.85	−85.82	−86.02	−86.36
$\Delta\xi$	0.0	796.14	10.23	4.19	4.39	4.73
PoH <sub>2</sub>	—	−290.25	−261.88	−91.58	−91.56	−91.79
H <sub>2</sub> O	—	−93.62	−6.45	−6.45	−7.47	−6.73
$\xi^{\text{tot}}$	−89.81	−383.87	−268.34	−98.03	−99.02	−98.52
$\Delta\xi$	0.0	294.06	178.53	8.22	9.21	8.71



metal clusters.[18] This curious additivity of magnetizability tensor – known as the Pascal’s rule[125, 126] – has been attributed to the local diamagnetic nature of atoms in molecules[124, 127] and the breakdown of this rule to the “*long-range circulation of electrons*” not accounted for in the atomic picture.[127]

While Pascal’s rule has been defined in terms of atomic susceptibilities, one could consider the additivity of magnetizability of molecular assemblies in terms of its constituent molecules. Recent studies[128] have shown that Pascal’s rule is particularly useful when analysed in terms of the magnetically induced current density, as the interaction of induced currents in neighbouring molecules and the increase of paramagnetic component of magnetizability tensor can be connected to the breakdown of the additivity rule.

### 1. Isolated subsystems

As can be seen in Table II, the  $\Delta\xi_{\text{iso}}^{\text{ME}}$  values are rather small in absolute ( $\pm 0.1$  for Se,  $-4.3$  for Te and  $-9.9$  for Po, in SI units) as well as in relative terms. From these results, one would be justified in considering that Pascal’s rule holds rather well for these systems.

The property shifts are larger for  $\xi_{\text{aniso1}}$ , with  $\Delta\xi_{\text{aniso1}}^{\text{ME}}$  that tend to increase with an increase of atomic number of X ( $-5.5$  for Se,  $4.7$  for Te and  $8.7$  for Po, in SI units) with the inverse trend for  $\Delta\xi_{\text{aniso2}}^{\text{ME}}$ . More interesting, however, is that these values amount overall to much larger relative differences ( $9.4\%$ ,  $-5.8\%$ ,  $-9.7\%$  for Se, Te and Po for  $\Delta\xi_{\text{aniso1}}^{\text{ME}}$ , respectively), and the change of sign along the series again indicates a complex interplay between relativistic and environmental effects in this sort of embedding.

### 2. Frozen Density Embedding

For magnetizability, FDE-LAO contributions are also present in the property gradient and in the expectation value part, thus it is again useful to consider the relative importance of each of them. We shall here once again focus on FDE(4) results, noting that FDE(0) results follow these closely but shows slightly worse agreement with supermolecular values than FDE(4). The  $\Delta\xi_{\text{iso}}^{\text{FDE(4)}}$  values calculated with no FDE-LAO terms are much larger in magnitude than those for the isolated calculations. Unlike for  $\sigma$ , even the inclusion of FDE-LAO[ $v$ ] terms yields  $\Delta\xi_{\text{iso}}^{\text{FDE(4)}}$  values which are significantly larger in magnitude ( $6.5$

for Se, 12 for Te and 80.3 for Po, in SI) than those for the isolated (“ME”) calculations.

The uncoupled kernel contribution ( $v + w_u$ ) brings about little changes in  $\Delta\xi_{\text{iso}}^{\text{FDE}(4)}$  for Se but significant improvement for Te and, especially, for Po. As for the NMR shielding, the coupling kernel ( $v + w_{\text{all}}$ ) term has a small effect, further leading to a decrease in the  $\Delta\xi_{\text{iso}}^{\text{FDE}(4)}$  values.

These results indicate that the additivity of  $\xi_{\text{iso}}$  results from FDE calculations with all second-order terms ( $v + w_{\text{all}}$ ) is significantly better than from the isolated (“ME”) calculations as the subsystem becomes heavier, and may suggest an inflexion point between Se and Te where electronic effects would become important enough for results to start deviating from Pascal’s rule.

A similar trend is found for the  $\Delta\xi_{\text{anisol}}^{\text{FDE}(4)}$  values, with FDE-LAO[ $v$ ] calculations underperforming isolated ones and the kernel contributions being important for yielding good agreement with reference values. As for the NMR shielding anisotropies, significant discrepancies with respect to the supermolecular results remain. The performance of FDE for the second anisotropy is slightly better but follows the same trends.

### C. NMR spin-spin coupling tensor

The indirect reduced spin-spin coupling tensor calculated with the DC Hamiltonian for the H–H<sub>b</sub>, X–H and X–H<sub>b</sub> pairs of nuclei corresponding to the XH<sub>2</sub> species are found in Table III.

#### 1. Isolated subsystems

The absolute values of isotropic one-bond spin-spin coupling constants (SSCCs) involving the heavy nuclei increase significantly and, due to relativity,[129] for PoH<sub>2</sub> are around 30 times larger to those in SeH<sub>2</sub>. In relative terms, however, X–H SSCCs hardly change for the isolated (“ME”) subsystems in relation to supermolecular values, with a slight increase as the systems become heavier (from about 2 for Se or Te to 5 for Po, SI units), whereas for X–H<sub>b</sub> SSCCs the opposite trend is found (from 7–9 for Se/Te to –1 for Po, SI units).

The observation that environment effects are more important in the case of Se–H<sub>b</sub> and Te–H<sub>b</sub> than of Se–H and Te–H, respectively, is intuitive considering that most of the studied

TABLE III. DC isotropic and anisotropic reduced indirect spin-spin couplings ( $K_{\text{iso}}^{\text{super}}$  and  $K_{\text{aniso}}^{\text{super}}$ , in SI) for the  $\text{H}_2\text{X}$  subsystem in  $\text{H}_2\text{X}-\text{H}_2\text{O}$ , and absolute shifts ( $\Delta K$ , in SI) for the isolated (“ME”) and embedded (“FDE(4)”)  $\text{H}_2\text{X}$  molecules in the presence of  $\text{H}_2\text{O}$ .

Nuclei	$K_{\text{iso}}^{\text{super}}$	$\Delta K_{\text{iso}}^{\text{FDE(4)}}$	$\Delta K_{\text{iso}}^{\text{ME}}$	$K_{\text{aniso}}^{\text{super}}$	$\Delta K_{\text{aniso}}^{\text{FDE(4)}}$	$\Delta K_{\text{aniso}}^{\text{ME}}$
$\text{H}_b$ Se	-11.22	1.52	7.25	113.79	-1.23	1.25
H Se	-16.04	0.07	1.51	110.68	-0.33	-1.01
$\text{H}_b$ H	-0.77	0.00	-0.02	0.89	0.00	-0.01
$\text{H}_b$ Te	-53.11	1.69	9.08	208.54	-0.42	8.07
H Te	-59.98	0.16	2.18	198.09	-0.44	-2.37
$\text{H}_b$ H	-0.75	0.00	-0.03	0.42	0.00	0.00
$\text{H}_b$ Po	-442.55	1.37	-1.25	429.17	3.10	41.96
H Po	-437.24	0.45	5.04	388.29	-0.18	2.24
$\text{H}_b$ H	-0.61	0.00	-0.04	0.69	0.00	1.32

one-bond spin-spin couplings are governed by Fermi contact interactions,[17] which probe the spin density at the coupled nuclei - expected to be perturbed more on  $\text{H}_b$  than on the other H nucleus upon formation of hydrogen bond. That said, the  $\Delta K_{\text{iso}}^{\text{ME}}(\text{Po}-\text{H}_b)$  value is interesting in being the only one which is negative and smaller than the  $\Delta K_{\text{iso}}^{\text{ME}}(\text{Po}-\text{H})$  value, something that may indicate that the spin-spin coupling mechanism in  $\text{PoH}_2$  molecule is more complex and may be dominated by other interactions, for instance spin-orbit-induced as in heavier interhalogen diatomics,[130] which may further be differently affected by environmental effects. Two-bond SSCs ( $\text{H}-\text{H}_b$ ) are in general very small for all systems, though there is a small increase in absolute terms as the systems become heavier.

For anisotropies, the values of  $\Delta K_{\text{aniso}}^{\text{ME}}$  strongly increase for  $\text{X}-\text{H}_b$  as X becomes heavier, though it remains very small for  $\text{X}-\text{H}$ , and for  $\text{H}-\text{H}_b$  isolated (“ME”) results are largely the same as supermolecular ones.

## 2. Frozen Density Embedding

Unlike the other two properties discussed above, FDE contributions to the response only enter here in the electronic Hessian, which greatly simplifies the implementation. Here we shall discuss SSCs FDE(4) results which are, like for magnetizabilities, better than FDE(0)

TABLE IV. Absolute SO-ZORA isotropic and anisotropic shielding values ( $\sigma_{\text{iso}}^{\text{super}}$  and  $\sigma_{\text{aniso}}^{\text{super}}$ , in ppm) of nuclei in  $\text{H}_2\text{X}$  ( $\text{X} = \text{Se}, \text{Te}, \text{Po}$ ) subsystems in  $\text{H}_2\text{X}-\text{H}_2\text{O}$ , and absolute shifts ( $\Delta\sigma$ , in ppm) for the isolated (“ME”) and embedded (“FDE(4)”)  $\text{H}_2\text{X}$  molecules in the presence of  $\text{H}_2\text{O}$ .

Atom	$\sigma_{\text{iso}}^{\text{super}}$	$\Delta\sigma_{\text{iso}}^{\text{FDE(4)}}$	$\Delta\sigma_{\text{iso}}^{\text{ME}}$	$\sigma_{\text{iso}}^{\text{super}}$	$\Delta\sigma_{\text{iso}}^{\text{FDE(4)}}$	$\Delta\sigma_{\text{iso}}^{\text{ME}}$
Se	2261.59	-11.30	34.89	628.15	4.43	4.89
H <sub>b</sub>	30.10	-0.77	-2.07	23.95	5.83	7.22
H	32.55	-0.03	0.35	16.97	-0.24	0.11
Te	4251.23	-9.61	64.66	1219.57	0.55	0.80
H <sub>b</sub>	33.43	-0.46	-1.59	18.09	3.87	4.90
H	35.47	0.00	0.45	13.09	-0.33	-0.09
Po	11168.82	-20.93	101.35	3138.04	-45.36	-304.56
H <sub>b</sub>	37.46	-0.21	-0.82	62.41	-1.32	-4.11
H	38.99	0.00	0.67	64.80	0.25	-2.05

results. We observe that FDE performs better than mechanical embedding, with  $\Delta K_{\text{iso}}^{\text{FDE(4)}}$  values being consistently around 1–2 ppm for  $\text{X}-\text{H}_b$  and smaller than 1 ppm for  $\text{X}-\text{H}$  or  $\text{H}-\text{H}_b$ .

Similar trends as for  $\Delta K_{\text{iso}}^{\text{FDE(4)}}$  are seen for  $\Delta K_{\text{aniso}}^{\text{FDE(4)}}$ , with the latter being generally small and slightly negative for all but  $\Delta K_{\text{aniso}}^{\text{FDE(4)}}(\text{Po}-\text{H}_b)$ , which is of about 3 (SI units).

#### D. A Comparison of DC and ZORA Hamiltonians

Although SO-ZORA is known to yield rather different results from DC ones, it is often sufficient in the determination of chemical shifts due to cancellation of errors.[21, 45] Nevertheless when environmental effects are calculated as differences of absolute shieldings, the cancellation of errors is not always guaranteed.

In recent years the differences in performance between the two Hamiltonians has gained attention, with a number of studies reporting significant discrepancies between SO-ZORA and DC values of NMR shielding tensors of heavy nuclei,[21, 22, 45, 131] which were explained by poor description of core orbitals of heavy elements by ZORA Hamiltonian.[21]

It is therefore interesting to see how FDE and ME perform for the two Hamiltonians. The results of our calculations of NMR shieldings and SSCs with SO-ZORA Hamiltonian

TABLE V. SO-ZORA isotropic and anisotropic reduced indirect spin-spin couplings ( $K_{\text{iso}}^{\text{super}}$  and  $K_{\text{aniso}}^{\text{super}}$ , in SI) for the  $\text{H}_2\text{X}$  subsystem in  $\text{H}_2\text{X}-\text{H}_2\text{O}$ , and absolute shifts ( $\Delta K$ , in SI) for the isolated (“ME”) and embedded (“FDE(4)”)  $\text{H}_2\text{X}$  molecules in the presence of  $\text{H}_2\text{O}$ .

Nuclei	$K_{\text{iso}}^{\text{super}}$	$\Delta K_{\text{iso}}^{\text{FDE(4)}}$	$\Delta K_{\text{iso}}^{\text{ME}}$	$K_{\text{aniso}}^{\text{super}}$	$\Delta K_{\text{aniso}}^{\text{FDE(4)}}$	$\Delta K_{\text{aniso}}^{\text{ME}}$
$\text{H}_b$ Se	-12.63	1.08	6.58	130.61	-2.01	1.15
H Se	-16.41	0.87	1.88	127.57	-0.24	-1.03
$\text{H}_b$ H	-1.11	-0.03	-0.07	-0.83	0.01	0.01
$\text{H}_b$ Te	-55.69	1.84	9.82	226.45	-1.00	8.95
H Te	-64.05	-0.02	1.44	214.87	-0.52	-2.61
$\text{H}_b$ H	-0.94	-0.02	-0.06	-0.34	0.00	0.00
$\text{H}_b$ Po	-439.33	1.02	-0.87	343.71	1.40	666.43
H Po	-435.42	0.40	4.12	-315.34	0.98	7.19
$\text{H}_b$ H	-0.80	-0.02	-0.07	0.78	0.00	0.08

are shown in Table IV and Table V, respectively.

A comparison of our SO-ZORA and DC results indicates that such error cancellation occurs for  $\text{SeH}_2$ , since the results and trends of shieldings and SSCCs are essentially the same for both Hamiltonians, for FDE and ME calculations. For  $\text{TeH}_2$  both Hamiltonians yield largely similar results, but some quantitative differences start to appear for  $\Delta\sigma_{\text{aniso}}$  and rather small differences for  $\Delta\sigma_{\text{iso}}^{\text{ME}}$ . For  $\text{PoH}_2$ , on the other hand, the differences are numerous:  $\Delta\sigma_{\text{iso}}^{\text{ME}}(\text{Po})$  for SO-ZORA already differs from DC value by 38 ppm, such difference for  $\Delta\sigma_{\text{iso}}^{\text{FDE(4)}}$  is about -16 ppm (DC using the  $(v + w_{\text{all}})$  FDE-LAO terms), whereas for  $\Delta\sigma_{\text{iso}}^{\text{ME}}(\text{H}_b)$  and  $\Delta\sigma_{\text{iso}}^{\text{FDE}}(\text{H}_b)$  these discrepancies are of the order of a ppm. The differences between Hamiltonians are also quite marked for anisotropies, where they amount to about 160 ppm for  $\Delta\sigma_{\text{aniso}}^{\text{ME}}(\text{Po})$  and 30 ppm for  $\Delta\sigma_{\text{aniso}}^{\text{FDE}}(\text{Po})$ .

Large discrepancies between Hamiltonians are also seen for  $\text{PoH}_2$  SSCCs, but much more marked for anisotropies than for isotropic values (about a ppm for FDE or ME calculations).

While our dataset is rather small for drawing more general conclusions, it strengthens the case for a more thorough assessment of approximate Hamiltonians such as ZORA for calculating NMR parameters of  $6p$  molecules.

## V. CONCLUSIONS AND OUTLOOK

In this paper we have described the implementation of frozen density embedding contributions in a response theory framework, in combination with four-component DC Hamiltonian to NMR indirect spin-spin couplings, NMR shieldings, and magnetizabilities for mean-field approaches (DFT-in-DFT or HF-in-DFT).

Due to the use of LAOs, which introduce the dependence of the electron- and spin-density on the external magnetic field in the case of NMR shieldings and magnetizabilities, additional embedding contributions to the property gradient (both properties) and expectation value (magnetizability only) arise, both for the individual subsystems as well as introducing a coupling between these.

By performing DFT calculations on  $\text{H}_2\text{X}-\text{H}_2\text{O}$  ( $\text{X} = \text{Se}, \text{Te}, \text{Po}$ ) model systems we have been able to show the relative importance of these additional contributions to the properties in question, while at the same time confirming the findings of other studies that frozen density embedding is well suited to the calculation of NMR indirect spin-spin couplings and NMR shieldings.

We have observed that the inclusion of the embedding potential in the FDE-LAO property gradient contributions accounts for the bulk of the environment effects, and that the heavier the center the more intra-subsystem FDE-LAO kernel contributions are important for both NMR shieldings and magnetizabilities, due to increasing importance of spin-density contributions. Coupling kernel LAO contributions, by contrast, are in general rather small.

We have exploited the use of the magnetically induced currents to obtain NMR shielding tensor via a real-space approach as well as to analyse, for the first time, the differences between supermolecular and embedded calculations in complement to the analysis of the electron density employed so far. We consider that the property density plots provide much clearer picture of where in space the deficiencies in the FDE treatment manifest themselves compared to scalar values of property shifts or unperturbed electron density plots as done prior to this work.

We present for the first time FDE contributions to magnetizabilities. Unlike the case of the electric polarizability and in line with Pascal’s rule, it appears that one can reconstruct to rather good accuracy the tensor for the supermolecular system from the tensors of the individual subsystems, obtained without the FDE coupling terms in the response equations.

This may potentially make FDE a more reliable route to obtaining molecular magnetizabilities than other embedding approaches, since the whole system is treated quantum-mechanically.

We have also compared our results to those obtained with the spin-orbit ZORA Hamiltonian. Although the latter performs well, for the  $\text{PoH}_2\text{--H}_2\text{O}$  system we have observed significantly different results between the Hamiltonians in the description of environment effects on the isotropic NMR shieldings and anisotropic spin-spin coupling constants. This is in contrast with the common expectation that relative shieldings are largely insensitive to changes in Hamiltonians and therefore it would be worthwhile to verify whether that is indeed the case for other systems containing the heaviest elements.

## VI. ACKNOWLEDGEMENTS

We would like to acknowledge inspiring discussions with Kenneth Ruud on the calculation of magnetizabilities, and with Christoph Jacob on the coupled response in FDE-NMR. We also acknowledge illuminating discussions with Michal Repisky on the question of magnetic balance in four-component calculations.

The members of the PhLAM laboratory acknowledge support from the CaPPA project (Chemical and Physical Properties of the Atmosphere), funded by the French National Research Agency (ANR) through the PIA (Programme d’Investissement d’Avenir) under contract “ANR-11-LABX-0005-01” as well as by the Ministry of Higher Education and Research, Hauts de France council and European Regional Development Fund (ERDF) through the Contrat de Projets Etat-Region (CPER) CLIMBIO (Changement climatique, dynamique de l’atmosphère, impacts sur la biodiversité et la santé humaine). Furthermore, ASPG acknowledges funding from the CNRS Institute of Physics (INP) via the PICS program (grant 6386), and computational time provided by the French national supercomputing facilities (grants DARI t2015081859, x2016081859).

## VII. APPENDIX: WORKING EXPRESSIONS FOR FDE-LAO CONTRIBUTIONS

In the DIRAC software, the quaternion algebra[132] is employed. Thus,  $\Omega_{pq;0}$  and  $i\Omega_{pq,\mu}$  are calculated from the real and imaginary parts, respectively, of the generally quaternion overlap distribution matrix (Eq. 12), what allows to easily discern charge- and spin-density

contributions to KS matrix and its derivatives.

Here we present the working formulas for FDE-LAO contributions to the property gradient (Eq. 43-45) and to the expectation value part of the magnetizability tensor (Eq. 49-50) derived for closed-shell reference. They were obtained by first separating the number-density ( $n$ :  $\rho_0 = -en$ ) and spin-density ( $s = \sqrt{\rho_\mu \cdot \rho_\mu}$ ,  $\mu \in \{x, y, z\}$ ) contributions, then by applying the local *ansatz*, in which XC and kinetic energies are approximated by functions of local density variables:[78]

$$E_{\text{xck}} = \int \epsilon_{\text{xck}}(Q^I \cup Q^{II}) d\vec{r}, \quad (70)$$

with  $Q^M = \{n^M, s^M, (\nabla n \cdot \nabla n)^M, (\nabla n \cdot \nabla s)^M, (\nabla s \cdot \nabla s)^M\}$  for  $M \in \{I, II\}$ . This allows to express the FDE-LAO contributions to the property gradient of subsystem I (the expression for subsystem II can be obtained by exchanging the labels  $I$  and  $II$ ) and to the expectation value part of the magnetizability tensor in terms of scalar and vector pre-factors ( $a_0, \vec{b}_0, c_0^{M,N}, c_\mu^{M,N}, \vec{d}_0^{M,N}, \vec{d}_\mu^{M,N}$  for  $M, N \in \{I, II\}$ ), summarized in Tables VII and VIII, while various perturbed densities are outlined in Table VI and discussed at length in literature.[40, 78, 133]



$$\begin{aligned}
\left. \frac{\partial}{\partial B_\alpha} \frac{\partial E_{\text{int}}}{\partial \kappa_{ai}^I} \right|_0 &= - \int \left[ a_0^{I, \check{\Omega}_{ia;0}^{B_\alpha;I}} + \vec{b}_0^I \cdot \nabla \check{\Omega}_{ia;0}^{B_\alpha;I} \right] d\vec{r} \\
&- \iint \left[ c_0^{I,I} \Omega_{ia;0}^I + \vec{d}_0^{I,I} \cdot \nabla \Omega_{ia;0}^I + c_\mu^{I,I} \Omega_{ia;\mu}^I + \sum_{\mu=x,y,z} \vec{d}_\mu^{I,I} \cdot \nabla \Omega_{ia;\mu}^I \right] d\vec{r}_1 d\vec{r}_2 \\
&- \iint \left[ c_0^{I,II} \Omega_{ia;0}^I + \vec{d}_0^{I,II} \cdot \nabla \Omega_{ia;0}^I + c_\mu^{I,II} \Omega_{ia;\mu}^I + \sum_{\mu=x,y,z} \vec{d}_\mu^{I,II} \cdot \nabla \Omega_{ia;\mu}^I \right] d\vec{r}_1 d\vec{r}_2
\end{aligned} \tag{71}$$

$$\begin{aligned}
\left. \frac{\partial^2 E_{\text{int}}}{\partial B_\alpha \partial B_\beta} \right|_0 &= \sum_{M=I,II} \left\{ \int \left[ a_0^{M, \check{\Omega}_{ii;0}^{B_\alpha B_\beta;M}} + \vec{b}_0^M \cdot \nabla \check{\Omega}_{ii;0}^{B_\alpha B_\beta;M} \right] d\vec{r} \right. \\
&+ \iint \left[ c_0^{M,M} \check{\Omega}_{ii;0}^{B_\beta;M} + \vec{d}_0^{M,M} \cdot \nabla \check{\Omega}_{ii;0}^{B_\beta;M} + c_\mu^{M,M} \check{\Omega}_{ii;\mu}^{B_\beta;M} + \sum_{\mu=x,y,z} \vec{d}_\mu^{M,M} \cdot \nabla \check{\Omega}_{ii;\mu}^{B_\beta;M} \right] d\vec{r}_1 d\vec{r}_2 \Big\} \\
&+ \sum_{\substack{M,N=I,II \\ M \neq N}} \iint \left[ c_0^{M,N} \check{\Omega}_{ii;0}^{B_\beta;M} + \vec{d}_0^{M,N} \cdot \nabla \check{\Omega}_{ii;0}^{B_\beta;M} + c_\mu^{M,N} \check{\Omega}_{ii;\mu}^{B_\beta;M} + \sum_{\mu=x,y,z} \vec{d}_\mu^{M,N} \cdot \nabla \check{\Omega}_{ii;\mu}^{B_\beta;M} \right] d\vec{r}_1 d\vec{r}_2.
\end{aligned} \tag{72}$$

$$\tag{73}$$

- 
- [1] Andrea Frank, Heiko M. Möller, and Thomas E. Exner. Toward the Quantum Chemical Calculation of NMR Chemical Shifts of Proteins. 2. Level of Theory, Basis Set, and Solvents Model Dependence. *J. Chem. Theory Comput.*, 8(4):1480, 2012.
- [2] Eric Oldfield. CHEMICAL SHIFTS IN AMINO ACIDS, PEPTIDES, AND PROTEINS: From Quantum Chemistry to Drug Design. *Annu. Rev. Phys. Chem.*, 53:349, 2002.
- [3] Joachim Bargon and Lars T. Kuhn. *In situ NMR Methods in Catalysis*, volume 276 of *Topics in Current Chemistry*. Springer-Verlag Berlin Heidelberg, 2007.
- [4] Jochen Autschbach. NMR Calculations for Paramagnetic Molecules and Metal Complexes. In David A. Dixon, editor, *Annual Reports in Computational Chemistry*, volume 11, page 3. Elsevier, 2015.
- [5] Guido Pintacuda and Gwendal Kervin. Paramagnetic solid-state magic-angle spinning nmr spectroscopy. In Henrike Heise and Stephen Matthews, editors, *Modern NMR Methodology*, volume 335 of *Topics in Current Chemistry*, page 157. Springer Berlin Heidelberg, 2013.
- [6] Laura Martel, J Somers, C Berkman, F Koepp, A Rothermel, O Pauvert, C Selfslag, and I Farnan. A nuclear magnetic resonance spectrometer concept for hermetically sealed magic

TABLE VI. The derivatives of the general density component,  $\rho_k$ , in OMO basis.  $\mathcal{P}_{\alpha\beta}$  denotes the permutation over indices  $\alpha$  and  $\beta$ ,  $k \in \{0, x, y, z\}$ . Basis functions labeled by  $\mu$  and  $\nu$  are centered on nuclei  $K$  and  $L$ , respectively. Subsystem indices are skipped. Second-order derivatives of overlap distribution involve the derivatives of LAO overlaps ( $\Omega_{ii;k}^{B_\alpha}$  and  $\Omega_{ii;k}^{B_\alpha B_\beta}$ ) and the brace notation of Helgaker and Jørgensen[134] and are discussed in details elsewhere.[135]

---

$$\left. \frac{\partial \rho_k}{\partial \kappa_{pq}} \right|_{\kappa=0} = -\Omega_{qp;k}$$

$$\left. \frac{\partial \rho_k}{\partial B_\alpha} \right|_{\vec{B}=0} = \check{\Omega}_{jj;k}^{B_\alpha}$$

$$\left. \frac{\partial^2 \rho_k}{\partial \kappa_{pq} \partial B_\alpha} \right|_{\vec{B}=0} = -\check{\Omega}_{qp;k}^{B_\alpha}$$

$$\left. \frac{\partial^2 \rho_k}{\partial B_\alpha \partial B_\beta} \right|_{\vec{B}=0} = \check{\Omega}_{jj;k}^{B_\alpha B_\beta}$$


---

$$\check{\Omega}_{pq;k}^{B_\alpha} = \frac{i\epsilon}{2} (\vec{R}_{KL} \times \vec{r})_\alpha c_{\mu p}^* c_{\nu q} \Omega_{\mu\nu;k} + \Omega_{\mu\nu;k} \left\{ c_{\mu t}^* T_{tp}^{B_\alpha} c_{\nu q} + c_{\mu p}^* c_{\nu t} T_{tq}^{B_\alpha} \right\}$$

$$\check{\Omega}_{ii;k}^{B_\alpha B_\beta} = \Omega_{ii;k}^{B_\alpha B_\beta} + \mathcal{P}_{\alpha\beta} \{T^\alpha, \Omega^{B_\beta}\}_{ii} + \{T^{B_\alpha B_\beta}, \Omega\}_{ii}$$

$$+ \frac{1}{2} \mathcal{P}_{\alpha\beta} (\{T^{B_\alpha}, \{T^{B_\beta}, \Omega\}\}_{ii} - \{T^{B_\beta} T^{B_\alpha}, \Omega\}_{ii;k})$$

angle spinning investigations on highly toxic , radiotoxic , or air sensitive materials A nuclear magnetic resonance spectrometer concept for hermetically sealed magic angle s. *Rev. Sci. Instrum.*, 84:055112, 2013.

- [7] H. Yasuoka, G. Koutroulakis, H. Chudo, S. Richmond, D. K. Veirs, A. I. Smith, E. D. Bauer, J. D. Thompson, G. D. Jarvinen, and D. L. Clark. Observation of  $^{239}\text{Pu}$  nuclear magnetic resonance. *Science*, 336(6083):901, 2012.
- [8] Trygve Helgaker, Sonia Coriani, Poul Jørgensen, Kasper Kristensen, Jeppe Olsen, and Kenneth Ruud. Recent Advances in Wave Function-Based Methods of Molecular-Property Calculations. *Chem. Rev.*, 112(1):543, 2012.
- [9] Trygve Helgaker, Michał Jaszuński, and Kenneth Ruud. Ab Initio Methods for the Calculation of NMR Shielding and Indirect Spin-Spin Coupling Constants. *Chem. Rev.*, 99(1):293, 1999.

TABLE VII. Scalar prefactors derived for closed-shell reference.  $a_0^I = v_{emb;0}^I$

$$\begin{aligned}
\vec{b}_0^I &= 2 \left( \frac{\partial \varepsilon_{xck}}{\partial (\nabla n \cdot \nabla n)} \Big|_{tot} \nabla n^{tot} - \frac{\partial \varepsilon_{xck}}{\partial (\nabla n \cdot \nabla n)} \Big|_I \nabla n^I \right) \\
c_0^{I,I} &= \left( \frac{\partial^2 \varepsilon_{xck}}{\partial n^2} \Big|_{tot} - \frac{\partial^2 \varepsilon_{xck}}{\partial n^2} \Big|_I \right) \check{\Omega}_{jj;0}^{I;B_\alpha} \\
&+ 2 \left( \frac{\partial^2 \varepsilon_{xck}}{\partial n \partial (\nabla n \cdot \nabla n)} \Big|_{tot} \cdot \nabla n^{tot} - \frac{\partial^2 \varepsilon_{xck}}{\partial n \partial (\nabla n \cdot \nabla n)} \Big|_I \cdot \nabla n^I \right) \cdot \nabla \check{\Omega}_{jj;0}^{I;B_\alpha} \\
\vec{d}_0^{I,I} &= 2 \left( \frac{\partial^2 \varepsilon_{xck}}{\partial n \partial (\nabla n \cdot \nabla n)} \Big|_{tot} \cdot \nabla n^{tot} - \frac{\partial^2 \varepsilon_{xck}}{\partial n \partial (\nabla n \cdot \nabla n)} \Big|_I \cdot \nabla n^I \right) \cdot \check{\Omega}_{jj;0}^{I;B_\alpha} \\
&+ 4 \left( \frac{\partial^2 \varepsilon_{xck}}{\partial (\nabla n \cdot \nabla n)^2} \Big|_{tot} \cdot \nabla n^{tot} \cdot \nabla n^{tot} - \frac{\partial^2 \varepsilon_{xck}}{\partial (\nabla n \cdot \nabla n)^2} \Big|_I \cdot \nabla n^I \cdot \nabla n^I \right) \cdot \nabla \check{\Omega}_{jj;0}^{I;B_\alpha} \\
&+ 2 \left( \frac{\partial \varepsilon_{xck}}{\partial (\nabla n \cdot \nabla n)} \Big|_{tot} - \frac{\partial \varepsilon_{xck}}{\partial (\nabla n \cdot \nabla n)} \Big|_I \right) \cdot \nabla \check{\Omega}_{jj;0}^{I;B_\alpha} \\
c_0^{I,II} &= \frac{\partial^2 \varepsilon_{xck}}{\partial n^2} \Big|_{tot} \check{\Omega}_{jj;0}^{II;B_\alpha} + \int \frac{1}{|\vec{r} - \vec{r}_1|} \check{\Omega}_{jj;0}^{II;B_\alpha}(\vec{r}_1) d\vec{r}_1 \\
&+ 2 \frac{\partial^2 \varepsilon_{xck}}{\partial n \partial (\nabla n \cdot \nabla n)} \Big|_{tot} \cdot \nabla n^{tot} \cdot \nabla \check{\Omega}_{jj;0}^{II;B_\alpha} \\
\vec{d}_0^{I,II} &= 2 \frac{\partial^2 \varepsilon_{xck}}{\partial n \partial (\nabla n \cdot \nabla n)} \Big|_{tot} \cdot \nabla n^{tot} \cdot \check{\Omega}_{jj;0}^{II;B_\alpha} \\
&+ 4 \frac{\partial^2 \varepsilon_{xck}}{\partial (\nabla n \cdot \nabla n)^2} \Big|_{tot} \cdot \nabla n^{tot} \cdot \nabla n^{tot} \cdot \nabla \check{\Omega}_{jj;0}^{II;B_\alpha} + 2 \frac{\partial \varepsilon_{xck}}{\partial (\nabla n \cdot \nabla n)} \Big|_{tot} \cdot \nabla \check{\Omega}_{jj;0}^{II;B_\alpha}
\end{aligned}$$

- [10] Julio C. Facelli. Chemical shift tensors: Theory and application to molecular structural problems. *Prog. Nucl. Mag. Res. Sp.*, 58(3-4):176, 2011.
- [11] Harden M. McConnell. Theory of Nuclear Magnetic Shielding in Molecules. I. LongRange

TABLE VIII. Vector prefactors derived for closed-shell reference.

$$\begin{aligned}
c_\mu^{I,I} &= \left( \frac{\partial^2 \varepsilon_{xck}}{\partial s^2} \Big|_{tot} - \frac{\partial^2 \varepsilon_{xck}}{\partial s^2} \Big|_I \right) \check{\Omega}_{jj;\mu}^{I;B_\alpha} \\
&+ \left( \frac{\partial^2 \varepsilon_{xck}}{\partial s \partial (\nabla n \cdot \nabla s)} \Big|_{tot} \cdot \nabla n^{tot} - \frac{\partial^2 \varepsilon_{xck}}{\partial s \partial (\nabla n \cdot \nabla s)} \Big|_I \cdot \nabla n^I \right) \cdot \nabla \check{\Omega}_{jj;\mu}^{I;B_\alpha} \\
\vec{d}_\mu^{I,I} &= \left( \frac{\partial^2 \varepsilon_{xck}}{\partial s \partial (\nabla n \cdot \nabla s)} \Big|_{tot} \cdot \nabla n^{tot} - \frac{\partial^2 \varepsilon_{xck}}{\partial s \partial (\nabla n \cdot \nabla s)} \Big|_I \cdot \nabla n^I \right) \cdot \check{\Omega}_{jj;\mu}^{I;B_\alpha} \\
&+ \left( \frac{\partial^2 \varepsilon_{xck}}{\partial (\nabla n \cdot \nabla s)^2} \Big|_{tot} \cdot \nabla n^{tot} \cdot \nabla n^{tot} - \frac{\partial^2 \varepsilon_{xck}}{\partial (\nabla n \cdot \nabla s)^2} \Big|_I \cdot \nabla n^I \cdot \nabla n^I \right) \cdot \nabla \check{\Omega}_{jj;\mu}^{I;B_\alpha} \\
&+ 2 \left( \frac{\partial \varepsilon_{xck}}{\partial (\nabla s \cdot \nabla s)} \Big|_{tot} - \frac{\partial \varepsilon_{xck}}{\partial (\nabla s \cdot \nabla s)} \Big|_I \right) \cdot \nabla \check{\Omega}_{jj;\mu}^{I;B_\alpha} \\
c_\mu^{I,II} &= \frac{\partial^2 \varepsilon_{xck}}{\partial s^2} \Big|_{tot} \check{\Omega}_{jj;\mu}^{II;B_\alpha} + \frac{\partial^2 \varepsilon_{xck}}{\partial s \partial (\nabla n \cdot \nabla s)} \Big|_{tot} \cdot \nabla n^{tot} \cdot \nabla \check{\Omega}_{jj;\mu}^{II;B_\alpha} \\
\vec{d}_\mu^{I,II} &= \frac{\partial^2 \varepsilon_{xck}}{\partial s \partial (\nabla n \cdot \nabla s)} \Big|_{tot} \cdot \nabla n^{tot} \cdot \check{\Omega}_{jj;\mu}^{II;B_\alpha} \\
&+ \frac{\partial^2 \varepsilon_{xck}}{\partial (\nabla n \cdot \nabla s)^2} \Big|_{tot} \cdot \nabla n^{tot} \cdot \nabla n^{tot} \cdot \nabla \check{\Omega}_{jj;\mu}^{II;B_\alpha} + 2 \frac{\partial \varepsilon_{xck}}{\partial (\nabla s \cdot \nabla s)} \Big|_{tot} \cdot \nabla \check{\Omega}_{jj;\mu}^{II;B_\alpha}
\end{aligned}$$

Dipolar Shielding of Protons. *J. Chem. Phys.*, 27(1):226, 1957.

- [12] Doree Sitkoff and David A. Case. Theories of chemical shift anisotropies in proteins and nucleic acids. *Prog. Nucl. Mag. Res. Sp.*, 32(2):165, 1998.
- [13] K. Jackowski and M. Jaszuński. *Gas Phase NMR*. New Developments in NMR. The Royal Society of Chemistry, 2016.
- [14] M. Kaupp, M. Buhl, and V. G. Malkin. *Calculation of NMR and EPR Parameters: Theory and Applications*. Wiley-VCH, 2004.
- [15] F. London. Théorie quantique des courants interatomiques dans les combinaisons aroma-

- tiques. *J. Phys. Radium*, 8(10):397, 1937.
- [16] Jochen Autschbach. Relativistic calculations of magnetic resonance parameters: background and some recent developments. *Phil. trans. R. Soc. A*, 372(2011):20120489, 2014.
  - [17] Michal Repisky, Stanislav Komorovsky, Radovan Bast, and Kenneth Ruud. Chapter 8 Relativistic Calculations of Nuclear Magnetic Resonance Parameters. In *Gas Phase NMR*, page 267. The Royal Society of Chemistry, 2016.
  - [18] Peter Schwerdtfeger, Behnam Assadollahzadeh, Urban Rohrmann, Rolf Schäfer, and James R. Cheeseman. Breakdown of the pseudopotential approximation for magnetizabilities and electric multipole moments: Test calculations for Au, AuF, and Snn cluster (n = 20). *J. Chem. Phys.*, 134(20):204102, 2011.
  - [19] Terutaka Yoshizawa and Masahiko Hada. Relativistic and electron-correlation effects on magnetizabilities investigated by the douglas-kroll-hess method and the second-order möller-plesset perturbation theory. *J. Comput. Chem.*, 30(15):2550, 2009.
  - [20] P. Pyykkö, A. Görling, and N. Rösch. A transparent interpretation of the relativistic contribution to the N.M.R. heavy atom chemical shift. *Mol. Phys.*, 61(1):195, 1987.
  - [21] Jochen Autschbach. The role of the exchange-correlation response kernel and scaling corrections in relativistic density functional nuclear magnetic shielding calculations with the zeroth-order regular approximation. *Mol. Phys.*, 111(16-17):2544, 2013.
  - [22] Jan Vicha, Jan Novotny, Michal Straka, Michal Repisky, Kenneth Ruud, Stanislav Komorovsky, and Radek Marek. Structure, solvent, and relativistic effects on the NMR chemical shifts in square-planar transition-metal complexes: assessment of DFT approaches. *Phys. Chem. Chem. Phys.*, 17:24944, 2015.
  - [23] S. Miertuš, E. Scrocco, and J. Tomasi. Electrostatic interaction of a solute with a continuum. a direct utilization of ab initio molecular potentials for the prevision of solvent effects. *Chem. Phys.*, 55(1):117, 1981.
  - [24] Maurizio Cossi, Nadia Rega, Giovanni Scalmani, and Vincenzo Barone. Energies, structures, and electronic properties of molecules in solution with the C-PCM solvation model. *J. Comput. Chem.*, 24(6):669, 2003.
  - [25] A. Klamt and G. Schuurmann. COSMO: a new approach to dielectric screening in solvents with explicit expressions for the screening energy and its gradient. *J. Chem. Soc., Perkin Trans. 2*, page 799, 1993.

- [26] C. Cory Pye and Tom Ziegler. An implementation of the conductor-like screening model of solvation within the Amsterdam density functional package. *Theor. Chem. Acc.*, 101(6):396, 1999.
- [27] A. S. P. Gomes and C. R. Jacob. Quantum-chemical embedding methods for treating local electronic excitations in complex chemical systems. *Annu. Rep. Prog. Chem., Sect. C: Phys. Chem.*, 108:222, 2012.
- [28] Christoph R. Jacob and Johannes Neugebauer. Subsystem density-functional theory. *Wiley Interdiscip Rev Comput Mol Sci*, 4(4):325, 2014.
- [29] Tomasz A. Wesolowski, Sapana Shedge, and Xiuwen Zhou. Frozen–Density Embedding Strategy for Multilevel Simulations of Electronic Structure. *Chem. Rev.*, 115(12):5891, 2015.
- [30] S. Höfener, A. S. P. Gomes, and L. Visscher. Molecular properties via a subsystem density functional theory formulation: a common framework for electronic embedding. *J. Chem. Phys.*, 136(4):044104, 2012.
- [31] Sebastian Höfener and Lucas Visscher. Calculation of electronic excitations using wave-function in wave-function frozen-density embedding. *J. Chem. Phys.*, 137(20):204120, 2012.
- [32] Sebastian Höfener, André Severo Pereira Gomes, and Lucas Visscher. Solvatochromic shifts from coupled-cluster theory embedded in density functional theory. *J. Chem. Phys.*, 139(10):104106, 2013.
- [33] Johannes Neugebauer. Couplings between electronic transitions in a subsystem formulation of time-dependent density functional theory. *J. Chem. Phys.*, 126(13):134116, 2007.
- [34] Johannes Neugebauer. On the calculation of general response properties in subsystem density functional theory. *J. Chem. Phys.*, 131(8):084104, 2009.
- [35] Andre Severo Pereira Gomes, Christoph R. Jacob, and Lucas Visscher. Calculation of local excitations in large systems by embedding wave-function theory in density-functional theory. *Phys. Chem. Chem. Phys.*, 10:5353, 2008.
- [36] Andre Severo Pereira Gomes, Christoph R. Jacob, Florent Real, Lucas Visscher, and Valerie Vallet. Towards systematically improvable models for actinides in condensed phase: the electronic spectrum of uranyl in  $\text{Cs}_2\text{UO}_2\text{Cl}_4$  as a test case. *Phys. Chem. Chem. Phys.*, 15:15153, 2013.
- [37] Rosa E. Buló, Christoph R. Jacob, and Lucas Visscher. NMR Solvent Shifts of Acetonitrile from Frozen Density Embedding Calculations. *J. Phys. Chem. A*, 112(12):2640, 2008.

- [38] C. R. Jacob and L. Visscher. Calculation of nuclear magnetic resonance shieldings using frozen-density embedding. *J. Chem. Phys.*, 125(19):194104, 2006.
- [39] Andreas W Götz, Jochen Autschbach, and Lucas Visscher. Calculation of nuclear spin-spin coupling constants using frozen density embedding. *J. Chem. Phys.*, 140(10):104107, 2014.
- [40] M. Olejniczak, R. Bast, T. Saue, and M. Pecul. A simple scheme for magnetic balance in four-component relativistic Kohn–Sham calculations of nuclear magnetic resonance shielding constants in a Gaussian basis. *J. Chem. Phys.*, 136(1):014108, 2012. Erratum: *ibid.* **136**, 239902, (2012).
- [41] Andrej Antusek and Martin Sulka. Ab initio calculations of NMR shielding of  $\text{Sc}^{3+}$ ,  $\text{Y}^{3+}$  and  $\text{La}^{3+}$  ions in the water solution and  $^{45}\text{Sc}$ ,  $^{89}\text{Y}$ ,  $^{138}\text{La}$  and  $^{139}\text{La}$  nuclear magnetic dipole moments. *Chem. Phys. Lett.*, 660:127, 2016.
- [42] Taye B. Demissie, Michal Jaszunski, Stanislav Komorovsky, Michal Repisky, and Kenneth Ruud. Absolute NMR shielding scales and nuclear spinrotation constants in  $^{175}\text{LuX}$  and  $^{197}\text{AuX}$  ( $X = ^{19}\text{F}$ ,  $^{35}\text{Cl}$ ,  $^{79}\text{Br}$  and  $^{127}\text{I}$ ). *J. Chem. Phys.*, 143(16):164311, 2015.
- [43] Stanislav Komorovsky, Michal Repisky, Elena Malkin, Kenneth Ruud, and Jurgen Gauss. Communication: The absolute shielding scales of oxygen and sulfur revisited. *J. Chem. Phys.*, 142(9):091102, 2015.
- [44] Perttu Lantto, Karol Jackowski, Włodzimierz Makulski, Małgorzata Olejniczak, and Michal Jaszunski. NMR Shielding Constants in  $\text{PH}_3$ , Absolute Shielding Scale, and the Nuclear Magnetic Moment of  $^{31}\text{P}$ . *J. Phys. Chem. A*, 115(38):10617, 2011.
- [45] Elena Malkin, Stanislav Komorovsky, Michal Repisky, Taye B. Demissie, and Kenneth Ruud. The Absolute Shielding Constants of Heavy Nuclei: Resolving the Enigma of the  $^{119}\text{Sn}$  Absolute Shielding. *J. Phys. Chem. Lett.*, 4(3):459, 2013.
- [46] G A Aucar, Trond Saue, Lucas Visscher, and H J Aa Jensen. On the origin and contribution of the diamagnetic term in four-component relativistic calculations of magnetic properties. *J. Chem. Phys.*, 110(13):6208, 1999.
- [47] M. Iliaš, T. Saue, T. Enevoldsen, and H. J. Aa. Jensen. Gauge origin independent calculations of nuclear magnetic shieldings in relativistic four-component theory. *J. Chem. Phys.*, 131(12):124119, 2009.
- [48] Miroslav Iliaš, Hans Jørgen Aa. Jensen, Radovan Bast, and Trond Saue. Gauge origin independent calculations of molecular magnetisabilities in relativistic four-component theory.

- Mol. Phys.*, 111(9–11):1373, 2013.
- [49] Thomas Enevoldsen, Lucas Visscher, Trond Saue, Hans Jrgen Aagaard Jensen, and Jens Oddershede. Relativistic four-component calculations of indirect nuclear spinspin couplings in  $MH_4$  ( $M=C, Si, Ge, Sn, Pb$ ) and  $Pb(CH_3)_3H$ . *J. Chem. Phys.*, 112(8):3493, 2000.
  - [50] Lucas Visscher, Thomas Enevoldsen, Trond Saue, Hans Jørgen Aagard Jensen, and Jens Oddershede. Full fourcomponent relativistic calculations of NMR shielding and indirect spinspin coupling tensors in hydrogen halides. *J. Comput. Chem.*, 20(12):1262, 1999.
  - [51] DIRAC, a relativistic ab initio electronic structure program, Release DIRAC15 (2015), written by R. Bast, T. Saue, L. Visscher, and H. J. Aa. Jensen, with contributions from V. Bakken, K. G. Dyall, S. Dubillard, U. Ekstroem, E. Eliav, T. Enevoldsen, E. Fasshauer, T. Fleig, O. Fossgaard, A. S. P. Gomes, T. Helgaker, J. Henriksson, M. Ilias, Ch. R. Jacob, S. Knecht, S. Komorovsky, O. Kullie, J. K. Laerdahl, C. V. Larsen, Y. S. Lee, H. S. Nataraj, M. K. Nayak, P. Norman, G. Olejniczak, J. Olsen, Y. C. Park, J. K. Pedersen, M. Pernpointner, R. Di Remigio, K. Ruud, P. Salek, B. Schimmelpfennig, J. Sikkema, A. J. Thorvaldsen, J. Thyssen, J. van Stralen, S. Villaume, O. Visser, T. Winther, and S. Yamamoto (see <http://www.diracprogram.org>).
  - [52] D. H. Whiffen. Expression of results in quantum chemistry. *Pure Appl. Chem.*, 50(1):75, 1978.
  - [53] Trond Saue. Relativistic Hamiltonians for chemistry: a primer. *ChemPhysChem*, 12(17):3077, 2011.
  - [54] K. G. Dyall and K. Faegri Jr. *Introduction to Relativistic Quantum Chemistry*. Oxford University Press, 2007.
  - [55] W. Kutzelnigg. Relativistic corrections to magnetic properties. *J. Comput. Chem.*, 20(12):1199, 1999.
  - [56] W. Kutzelnigg. Diamagnetism in relativistic theory. *Phys. Rev. A*, 67(3):032109, 2003.
  - [57] L. Visscher. Magnetic Balance and Explicit Diamagnetic Expressions for Nuclear Magnetic Resonance Shielding Tensors. *Adv. Quantum Chem.*, 48:369, 2005.
  - [58] S. Komorovský, M. Repiský, O. L. Malkina, V. G. Malkin, I. Malkin Ondík, and M. Kaupp. A fully relativistic method for calculation of nuclear magnetic shielding tensors with a restricted magnetically balanced basis in the framework of the matrix Dirac–Kohn–Sham equation. *J. Chem. Phys.*, 128(10):104101, 2008.



- [59] S. Komorovsky, M. Repisky, O. L. Malkina, and V. G. Malkin. Fully relativistic calculations of NMR shielding tensors using restricted magnetically balanced basis and gauge including atomic orbitals. *J. Chem. Phys.*, 132(15):154101, 2010.
- [60] M. Repisky, S. Komorovsky, O. L. Malkina, and V. G. Malkin. Restricted magnetically balanced basis applied for relativistic calculations of indirect nuclear spin-spin coupling tensors in the matrix Dirac-Kohn-Sham framework. *Chem. Phys.*, 356(1-3):236, 2009.
- [61] L. Cheng, Y. Xiao, and W. Liu. Four-component relativistic theory for nuclear magnetic shielding: Magnetically balanced gauge-including atomic orbitals. *J. Chem. Phys.*, 131(24):244113, 2009.
- [62] R. D. Reynolds and T. Shiozaki. Fully relativistic self-consistent field under a magnetic field. *Phys. Chem. Chem. Phys.*, 17(22):14280, 2015.
- [63] J. Olsen, K. L. Bak, K. Ruud, T. Helgaker, and P. Jørgensen. Orbital connections for perturbation-dependent basis sets. *Theor. Chem. Acc.*, 90(5-6):421, 1995.
- [64] Christoph R. Jacob and Markus Reiher. Spin in Density-Functional Theory. *Int. J. Quant. Chem.*, 112(23):3661, 2012.
- [65] A. K. Rajagopal and J. Callaway. Inhomogeneous electron gas. *Phys. Rev. B*, 7:1912, 1973.
- [66] U. von Barth and L. Hedin. A local exchange-correlation potential for the spin polarized case. i. *J. Phys. C Solid State Phys.*, 5:1629, 1972.
- [67] G Vignale and M. Rasolt. Density-functional theory in strong magnetic fields. *Phys. Rev. Lett.*, 59(20):2360, 1987.
- [68] G. Vignale and M. Rasolt. Current- and spin-density-functional theory for inhomogeneous electronic systems in strong magnetic fields. *Phys. Rev. B*, 37(18):10685, 1988.
- [69] G. Vignale, Mark Rasolt, and D. J. W. Geldart. Diamagnetic susceptibility of a dense electron gas. *Phys. Rev. B*, 37:2502, 1988.
- [70] James W. Furness, Joachim Verbeke, Erik I. Tellgren, Stella Stopkiewicz, Ulf Ekström, Trygve Helgaker, and Andrew M. Teale. Current Density Functional Theory Using Meta-Generalized Gradient Exchange-Correlation Functionals. *J. Chem. Theory Comput.*, 11(9):4169, 2015.
- [71] Aaron M. Lee, Susan M. Colwell, and Nicholas C. Handy. The calculation of magnetisabilities using current density functional theory. *Chem. Phys. Lett.*, 229(3):225, 1994.
- [72] Aaron M. Lee, Nicholas C. Handy, and Susan M. Colwell. The density functional calculation of nuclear shielding constants using London atomic orbitals. *J. Chem. Phys.*, 103(23):10095,

- 1995.
- [73] E. I. Tellgren, A. M. Teale, J. W. Furness, K. K. Lange, U. Ekström, and T. Helgaker. Non-perturbative calculation of molecular magnetic properties within current-density functional theory. *J. Chem. Phys.*, 140(3):034101, 2014.
  - [74] Ola B. Lutnaes, Andrew M. Teale, Trygve Helgaker, David J. Tozer, Kenneth Ruud, and Jürgen Gauss. Benchmarking density-functional-theory calculations of rotational g tensors and magnetizabilities using accurate coupled-cluster calculations. *J. Chem. Phys.*, 131(14):144104, 2009.
  - [75] Andrew M. Teale, Ola B. Lutnaes, Trygve Helgaker, David J. Tozer, and Jürgen Gauss. Benchmarking density-functional theory calculations of NMR shielding constants and spin-rotation constants using accurate coupled-cluster calculations. *J. Chem. Phys.*, 138(2):024111, 2013.
  - [76] E. Engel. Chapter 10. Relativistic density functional theory: foundation and basic formalism. In P. Schwerdtfeger, editor, *Relativistic Electronic Structure Theory*, volume 11 of *Theoretical and Computational Chemistry*, page 523. Elsevier, 2002.
  - [77] E. Engel and R. M. Dreizler. *Density Functional Theory. An Advanced Course*. Theoretical and Mathematical Physics. Springer Berlin Heidelberg, 2011.
  - [78] R. Bast, H. J. Aa. Jensen, and T. Saue. Relativistic adiabatic time-dependent density functional theory using hybrid functionals and noncollinear spin magnetization. *Int. J. Quant. Chem.*, 109(10):2091, 2009.
  - [79] T. Saue and H. J. Aa. Jensen. Linear response at the 4-component relativistic level: Application to the frequency-dependent dipole polarizabilities of the coinage metal dimers. *J. Chem. Phys.*, 118(2):522, 2003.
  - [80] Alisa Solovyeva, Michele Pavanello, and Johannes Neugebauer. Spin densities from subsystem density-functional theory: Assessment and application to a photosynthetic reaction center complex model. *J. Chem. Phys.*, 136(19):194104, 2012.
  - [81] Tomasz Adam Wesolowski and Jacques Weber. *Recent Advances in Density Functional Methods*, chapter 24, page 371. World Scientific, 2002.
  - [82] T. A. Wesolowski and A. Warshel. Frozen density functional approach for ab initio calculations of solvated molecules. *J. Phys. Chem.*, 97(30):8050, 1993.
  - [83] Christoph R. Jacob, Johannes Neugebauer, and Lucas Visscher. A flexible implementation

- of frozen-density embedding for use in multilevel simulations. *J. Comput. Chem.*, 29(6):1011, 2008.
- [84] Danny Schlüns, Kevin Klahr, Christian Mück-Lichtenfeld, Lucas Visscher, and Johannes Neugebauer. Subsystem-DFT potential-energy curves for weakly interacting systems. *Phys. Chem. Chem. Phys.*, 17:14323, 2015.
- [85] Denis G. Artiukhin, Christoph R. Jacob, and Johannes Neugebauer. Excitation energies from frozen-density embedding with accurate embedding potentials. *J. Chem. Phys.*, 142(23):234101, 2015.
- [86] Samuel Fux, Christoph R. Jacob, Johannes Neugebauer, Lucas Visscher, and Markus Reiher. Accurate frozen-density embedding potentials as a first step towards a subsystem description of covalent bonds. *J. Chem. Phys.*, 132(16):164101, 2010. Comment: T. A. Wesolowski, *ibid.* **135**, 027101, (2011). Response: S. Fux, C. R. Jacob, J. Neugebauer and M. Reiher, *ibid.* **135**, 027102, (2011).
- [87] Jan P. Unsleber, Johannes Neugebauer, and Christoph R. Jacob. No need for external orthogonality in subsystem density-functional theory. *Phys. Chem. Chem. Phys.*, 18(31):21001, 2016.
- [88] Sebastian Höfener and Lucas Visscher. Wave Function Frozen-Density Embedding: Coupled Excitations. *J. Chem. Theory Comput.*, 12(2):549, 2016.
- [89] Michele Pavanello. On the subsystem formulation of linear-response time-dependent DFT. *J. Chem. Phys.*, 138(20):204118, 2013.
- [90] Johannes Neugebauer and Evert Jan Baerends. Exploring the Ability of Frozen-Density Embedding to Model Induced Circular Dichroism. *J. Phys. Chem. A*, 110(28):8786, 2006.
- [91] Johannes Neugebauer, Christoph R. Jacob, Tomasz A. Wesolowski, and Evert Jan Baerends. An Explicit Quantum Chemical Method for Modeling Large Solvation Shells Applied to Aminocoumarin C151. *J. Phys. Chem. A*, 109(34):7805, 2005.
- [92] Johannes Neugebauer, Manuel J. Louwerse, Evert Jan Baerends, and Tomasz A. Wesolowski. The merits of the frozen-density embedding scheme to model solvatochromic shifts. *J. Chem. Phys.*, 122(9):094115, 2005.
- [93] R. Bast, J. Jusélius, and T. Saue. 4-Component relativistic calculation of the magnetically induced current density in the group 15 heteroaromatic compounds. *Chem. Phys.*, 356(1–3):187–194, 2009.

- [94] Cynthia J. Jameson and A. D. Buckingham. Molecular electronic property density functions: The nuclear magnetic shielding density. *J. Chem. Phys.*, 73(11):5684, 1980.
- [95] David Sulzer, Małgorzata Olejniczak, Radovan Bast, and Trond Saue. 4-Component relativistic magnetically induced current density using London atomic orbitals. *Phys. Chem. Chem. Phys.*, 13:20682, 2011.
- [96] ADF2014, SCM, Theoretical Chemistry, Vrije Universiteit, Amsterdam, The Netherlands, <http://www.scm.com>.
- [97] E. van Lenthe, E. J. Baerends, and J. G. Snijders. Relativistic regular twocomponent Hamiltonians. *J. Chem. Phys.*, 99(6):4597, 1993.
- [98] E. van Lenthe, E. J. Baerends, and J. G. Snijders. Relativistic total energy using regular approximations. *J. Chem. Phys.*, 101(11):9783, 1994.
- [99] A. D. Becke. Density-functional thermochemistry. III. The role of exact exchange. *J. Chem. Phys.*, 98(7):5648, 1993.
- [100] E. Van Lenthe and E. J. Baerends. Optimized slater-type basis sets for the elements 1–118. *J. Comput. Chem.*, 24(9):1142, 2003.
- [101] John P. Perdew, Kieron Burke, and Matthias Ernzerhof. Generalized Gradient Approximation Made Simple. *Phys. Rev. Lett.*, 77:3865, Oct 1996.
- [102] John P. Perdew, Kieron Burke, and Matthias Ernzerhof. Generalized Gradient Approximation Made Simple [Phys. Rev. Lett. 77, 3865 (1996)]. *Phys. Rev. Lett.*, 78:1396, Feb 1997.
- [103] A. Lembarki and H. Chermette. Obtaining a gradient-corrected kinetic-energy functional from the perdew-wang exchange functional. *Phys. Rev. A*, 50:5328, Dec 1994.
- [104] Ulf Ekström, Lucas Visscher, Radovan Bast, Andreas J. Thorvaldsen, and Kenneth Ruud. Arbitrary-order density functional response theory from automatic differentiation. *J. Chem. Theory Comput.*, 6(7):1971, 2010.
- [105] T. H. Dunning. Gaussian basis sets for use in correlated molecular calculations. I. The atoms boron through neon and hydrogen. *J. Chem. Phys.*, 90(2):1007, 1989.
- [106] G. Kenneth Dyall. Relativistic and nonrelativistic finite nucleus optimized triple-zeta basis sets for the 4p, 5p and 6p elements. *Theor. Chem. Acc.*, 108(6):335, 2002. The basis sets are available from the DIRAC web site <http://dirac.chem.sdu.dk>.
- [107] Kenneth G. Dyall. Relativistic Quadruple-Zeta and Revised Triple-Zeta and Double-Zeta Basis Sets for the 4p, 5p, and 6p Elements. *Theor. Chem. Acc.*, 115(5):441, 2006. The basis

- sets are available from the DIRAC web site <http://dirac.chem.sdu.dk>.
- [108] L. Visscher and K. G. Dyall. Dirac–Fock atomic electronic structure calculations using different nuclear charge distributions. *Atomic Data and Nuclear Data Tables*, 67(2):207, 1997. see also <http://www.few.vu.nl/~visscher/FiniteNuclei/FiniteNuclei.htm>.
  - [109] L. Visscher. Approximate molecular relativistic Dirac–Coulomb calculations using a simple Coulombic correction. *Theor. Chem. Acc.*, 98:68, 1997.
  - [110] J. Mason. Conventions for the reporting of nuclear magnetic shielding (or shift) tensors suggested by participants in the NATO ARW on NMR shielding constants at the University of Maryland, College Park, July 1992. *Solid State Nucl Magn Reson*, 2(5):285, 1993.
  - [111] P. Ramachandran and G. Varoquaux. Mayavi: 3D Visualization of Scientific Data. *Computing in Science & Engineering*, 13(2):40, 2011.
  - [112] E. Arunan, G. Desiraju, R. Klein, J. Sadlej, S. Scheiner, I. Alkorta, D. C. Clary, R. H. Crabtree, J. J. Dannenberg, Hobza. P., H. G. Kjaergaard, A. C. Legon, B. Mennucci, and D. J. Nesbitt. Definition of the hydrogen bond (IUPAC Recommendations 2011). *Pure and Applied Chemistry*, 83(8):1637, 2011.
  - [113] Narendra P. Luthra and Jerome D. Odom. *Nuclear magnetic resonance and electron spin resonance studies of organic selenium and tellurium compounds*, page 189. John Wiley & Sons, Inc., 2010.
  - [114] Helmut Dudgeon. <sup>77</sup>Se NMR Spectroscopy and Its Applications in Chemistry. volume 52 of *Annual Reports on NMR Spectroscopy*, page 105. Academic Press, 2004.
  - [115] T.F. Kemp, A. Wong, M.E. Smith, P.T. Bishop, and N. Carthey. A natural abundance <sup>77</sup>Se solid-state NMR study of inorganic compounds. *Solid State Nuclear Magnetic Resonance*, 34(4):224, 2008.
  - [116] Satoko Hayashi, Kohei Matsuiwa, and Waro Nakanishi. Relativistic effects on the <sup>125</sup>Te and <sup>33</sup>S NMR chemical shifts of various tellurium and sulfur species, together with <sup>77</sup>Se of selenium congeners, in the framework of a zeroth-order regular approximation: applicability to tellurium compounds. *RSC Adv.*, 4:44795, 2014.
  - [117] Yury Yu. Rusakov and Leonid B. Krivdin. Four-component relativistic dft calculations of <sup>77</sup>se nmr chemical shifts: A gateway to a reliable computational scheme for the medium-sized organoselenium molecules. *J. Comput. Chem.*, 36(23):1756, 2015.
  - [118] Yury Yu. Rusakov, Irina L. Rusakova, and Leonid B. Krivdin. Mp2 calculation of <sup>77</sup>se nmr

- chemical shifts taking into account relativistic corrections. *Magn Reson Chem.*, 53(7):485, 2015.
- [119] <http://dx.doi.org/10.5281/zenodo.179667>. Figures available under a CC-BY 4.0 license.
- [120] Jochen Autschbach. Chapter 4 - Relativistic Effects on NMR Parameters. In Rubén H. Contreras, editor, *High Resolution NMR Spectroscopy. Understanding Molecules and their Electronic Structures*, volume 3 of *Science and Technology of Atomic, Molecular, Condensed Matter & Biological Systems*, page 69. Elsevier, 2013.
- [121] Per-Olof Astrand and Kurt V. Mikkelsen. Atomic magnetizability tensors of benzene and fluoro- and chlorobenzenes. *Magn Reson Chem.*, 36(2):92, 1998.
- [122] Richard F. W. Bader and Todd A. Keith. Properties of atoms in molecules: Magnetic susceptibilities. *J. Chem. Phys.*, 99(5):3683, 1993.
- [123] Kenneth Ruud, Haakon Skaane, Trygve Helgaker, Keld L. Bak, and Poul Jørgensen. Magnetizability of Hydrocarbons. *J. Am. Chem. Soc.*, 116(22):10135, 1994.
- [124] Kenneth Ruud, Per-Olof Astrand, and Peter R. Taylor. Molecular Magnetizabilities: Zero-Point Vibrational Effects and the Breakdown of Pascal’s Rule. *J. Phys. Chem. A*, 105(43):9926, 2001.
- [125] P. Pascal. *Ann. Chim. Phys.*, 19:5, 1910.
- [126] P. Pascal. *Rev. Sci. Instrum.*, 86:38, 1948.
- [127] W. H. Flygare. Magnetic interactions in molecules and an analysis of molecular electronic charge distribution from magnetic parameters. *Chem. Rev.*, 74(6):653, 1974.
- [128] Kenneth Ruud, private communication.
- [129] J. Autschbach and S. Zheng. Chapter 1 Relativistic Computations of NMR Parameters from First Principles: Theory and Applications. In Graham A. Webb, editor, *Annual Reports on NMR Spectroscopy*, volume 67 of *Annual Reports on NMR Spectroscopy*, page 1. Academic Press, 2009.
- [130] David L. Bryce, Roderick E. Wasylishen, Jochen Autschbach, and Tom Ziegler. Periodic Trends in Indirect Nuclear SpinSpin Coupling Tensors: Relativistic Density Functional Calculations for Interhalogen Diatomics. *J. Am. Chem. Soc.*, 124(17):4894, 2002.
- [131] Wlodzimierz Makulski. Tetramethyltin study by NMR spectroscopy in the gas and liquid phase. *J. Mol. Struct. (Theochem)*, 1017:45, 2012.
- [132] T. Saue and H. J. Aa. Jensen. Quaternion symmetry in relativistic molecular calculations:

- The Dirac–Hartree–Fock method. *J. Chem. Phys.*, 111(14):6211, 1999.
- [133] P. Sałek, T. Helgaker, and T. Saue. Linear response at the 4-component relativistic density-functional level: application to the frequency-dependent dipole polarizability of Hg, AuH and PtH. *Chem. Phys.*, 311(1-2):187, 2005.
- [134] T. Helgaker and P. Jørgensen. An electronic Hamiltonian for origin independent calculations of magnetic properties. *J. Chem. Phys.*, 95(4):2595, 1991.
- [135] M. Olejniczak and T. Saue, in preparation.